Physics – Uspekhi **57** (6) 527 – 555 (2014)

REVIEWS OF TOPICAL PROBLEMS PACS numbers: 04.50.Gh, 11.25.Tq, 12.38.Mh, **24.85.+p**

Holographic approach to quark–gluon plasma in heavy ion collisions

I Ya Aref'eva

DOI: 10.3367/UFNe.0184.201406a.0569

Contents

Abstract. We review recent applications of the dual holographic approach to describing the quark–gluon plasma observed in high-energy collisions of relativistic heavy nuclei. Holography and AdS/CFT duality provide a means to study the properties of strong-coupling quantum field theories using higher-dimensional gravity theories. The appearance of quark–gluon plasma in heavy ion collisions can be described in dual terms as the formation of a black hole. To illustrate the major achievements of holographic theory, we discuss the calculation of the following quantities: the shear viscosity and other transport coefficients (all calculated by second order hydrodynamic models), the energy dependence of multiplicities, and the anisotropic thermalization and isotropization times. We also compare theoretical predictions with available experimental data, including the recent LHC results.

I Ya Aref'eva Steklov Mathematical Institute,
Russian Academy of Sciences,
ul. Gubkina 8, 119991 Moscow, Russian Federation
E-mail: arefeva@mi.ras.ru

Received 26 May 2013, revised 5 July 2013
Uspekhi Fizicheskikh Nauk **184** (6) 569 – 598 (2014)
DOI: 10.3367/UFNr.0184.201406a.0569
Translated by Yu V Morozov; edited by A Radzig

1. Introduction

Quark–gluon plasma that is a new state of matter was discovered in 2005 in heavy-ion collision experiments [1–5]. It is assumed that the evolving Universe was in this state after a short span of time (of order 10^{-11} s) following the Big Bang.

There are many attempts to describe the quark–gluon plasma (QGP) formed in heavy ion collisions in the framework of quantum chromodynamics (QCD) [16–19]. The main problem with such attempts is that they require calculating time-dependent correlation functions in a strong coupling regime.

In recent years, a promising new approach has been developed in the QGP theory taking advantage of holographic duality of a quantum-field system in a strong coupling regime in the four-dimensional Minkowski space and classical gravity in the five-dimensional bulk anti-de Sitter (AdS) space [20–23]. Specifically, considerable progress has been achieved in the holographic description of equilibrium QGP [24]. The holographic approach is successfully applied to the QGP formation process. In terms of this approach, QGP thermalization is perfectly described as the formation of a black hole in AdS space, and the multiplicity of newly-created particles is related to black hole entropy. The present review is designed to discuss recent results on the use

of the dual holographic description of QGP produced in heavy nucleus collisions at high energies.

The current concept of QGP formation and evolution in outline coincides with that of multiparticle production in high-energy particle collisions proposed in the classical works of Fermi and Landau [25–27]. A characteristic feature of the Landau theory is that it includes thermodynamic considerations at the early stage of plasma formation and the hydrodynamic approach to the description of its further evolution. Such a picture makes up the approximation to a more complete representation of the respective processes, in particular, based on the holographic approach which allows describing

- the thermalization process in heavy ion collisions;
- properties of equilibrium QGP produced in such collisions;
- a hydrodynamic approximation free of the problems arising from the break in causality.

Holographic duality establishes the relationship between the nonequilibrium quantum theory in a 4-dimensional bulk spacetime in the strong interaction regime and 5-dimensional classical gravity for the times immediately after high-energy particle collision, and the relationship between two classical theories (4-dimensional hydrodynamics and 5-dimensional classical gravity) for later times. The transition regime from the nonequilibrium 4-dimensional quantum theory to hydrodynamics suggests a consistent description in the framework of unified 5-dimensional classical gravity. Due to duality, the 4-dimensional quantum problem of QGP formation reduces (in the approximation being considered) to the classical problem of the general relativity theory (GR) in the 5-dimensional bulk. Having solved this 5-dimensional problem yields a sufficiently complete holographic picture of QGP formation.

There are two problems here. One arises from the fact that the corresponding GR problems are rather complicated. Considerable progress has recently been achieved in the study of solutions with special symmetry. Based on Bjorken's arguments concerning the ultrarelativistic character of particle collisions, it is possible to consider a class of boost-invariant solutions in the 5-dimensional spacetime. The numerical analysis for this class is significantly simplified. The results of calculations suggest local anisotropic thermalization in the 4-dimensional theory with corresponding holographic duality. Transition to the isotropic state can be followed up in both holographic and hydrodynamic approaches leading to virtually identical results, thus demonstrating common hydrodynamic/gravity duality.

The other problem is related to the necessity of modifying the fact that the holographic model itself. It arises, strictly speaking, from the fact that the duality is established between supergravity in 5-dimensional AdS space and the conformally invariant gauge theory in the 4-dimensional Minkowski space; to be precise, there is a duality between the $\mathcal{N} = 4$ supersymmetric Yang–Mills theory with matter fields in the adjoint representation of the $\mathrm{SU}(N_\mathrm{c})$ gauge group with the number of colors $N_\mathrm{c} \to \infty$ and the IIB superstring theory in $\mathrm{AdS}_5 \times \mathrm{S}^5$ space, i.e., the direct product of anti-de-Sitter space and a 5-dimensional sphere. Quantum chromodynamics is not a supersymmetry theory; the gauge color group in QCD is SU(3) even if the 't Hooft limit as $N_\mathrm{c} \to \infty$ reproduces a number of phenomenologically acceptable properties (see, for instance, report [28]); matter fields in QCD undergo transformation in accordance with the fundamental representation and have, in addition, a flavor; moreover, there is no conformal invariance in QCD. However, certain QCD characteristics at high temperatures become close to those of the $\mathcal{N} = 4$ supersymmetric Yang–Mills theory: lattice calculations show that QCD acquires properties of conformal theory; on the other hand, the results of calculations in the $\mathcal{N} = 4$ supersymmetric Yang–Mills theory for collective excitations with the help of the Keldysh diagram technique indicate that its supersymmetry properties gradually disappear.

A more accurate holographic description suggests modification of the dual model by building so-called improved holographic models that include not only gravity but also the lowest string scalar mode, dilaton. Thus far, these models have been applied to describe properties of stationary QGP (see Section 5.6). It is interesting to trace how such modification affects characteristics of the QGP formation process. It turns out that specifically holographic models associated with background solutions describing stationary QGP properties equally well describe the multiplicity obtained in recent experiments at the Large Hadron Collider (LHC). These models are extensively analyzed in ongoing research.

The layout of the review is as follows.

Section 2 is designed to discuss the main characteristics of QGP and analogies between characteristics of QGP producing in heavy ion collisions and QGP in the early Universe.

Section 3 presents some results of experiments on heavy ion collisions in accelerators. These experimental data are compared in Sections 5–7 with the results of the theoretical holographic approach. A more comprehensive description of the experimental results and their alternative explanations can be found, for instance, in reviews [13, 18, 29–31] (see also relevant references in Sections 2–4).

Section 4 contains concise hydrodynamic description of QGP and the main features of Landau and Bjorken models; also discussed are problems encountered in the theory of a relativistic viscous fluid.

Section 5 is focused on the main concepts of the holographic approach to describing equilibrium QGP. The AdS/CFT correspondence (CFT — conformal field theory) is illustrated by simple examples. The optical approximation incorporated calculation of geodesics in the 5-dimension bulk is used to calculate two-point correlators both in a vacuum and at a nonzero temperature. These calculations provide a basis for the holographic search for more complex correlators. As mentioned above, considerable progress has been achieved in holographic descriptions of the properties of stationary QGP, viz. viscosity, energy losses, quarkonium spectrum, etc. Section 5.6 reports the results of these calculations for so-called improved holographic QCD models. In this context, AdS/QCD correspondence is also commonly broached.

Results of the holographic approach to thermalization of quantum systems are presented in Section 6. A few models of holographic thermalization are considered. An effective model of holographic thermalization is that of light-like shells thrown into the 5-dimensional AdS space. Such models make it possible to quantitatively characterize the processes of thermalization of nonlocal quantities and elucidate their dependence on general characteristics, such as thermalization temperature and chemical potential. Another model of holographic thermalization is also built in which colliding ions are described in the dual picture by gravitational shock waves in the background AdS space. The formation of a black

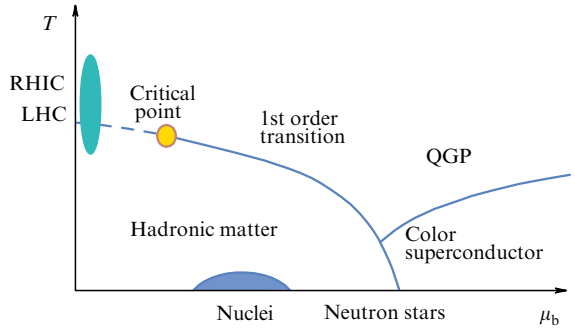

Figure 1. (Color online.) QCD phase diagram.

hole corresponds to the formation of a trapped surface. In the dual language, multiplicity of particles produced in ion collisions is estimated as the trapped surface area formed in shock wave collisions in the 5-dimensional bulk.

Gravity/hydrodynamics duality is described in Section 7, where equations of relativistic conformal hydrodynamics with dissipation up to a second order of smallness in gradients and calculated transfer coefficients are presented.

The formulas of relativistic hydrodynamics used in the review and the description of AdS geometry are given in the Appendices.

2. Quark–gluon plasma: a new state of matter

2.1 Main characteristics of quark–gluon plasma

QGP is a state of matter formed by free quarks, antiquarks, and gluons at a high temperature. As is well-known, quark–gluon interaction is described by QCD with its quark confinement and asymptotic freedom. It is also known (mainly from lattice calculations [32]) that matter passes into the deconfinement phase with increasing nuclear matter temperature T or energy density ε.

The QCD phase diagram has up to now been poorly investigated both theoretically and experimentally. The generally accepted hypothetical form of the phase diagram in the (quark chemical potential[1] μ_b–temperature T) variables is depicted in Fig. 1 (see, for instance, review [17]).

There is a critical point at $T \sim 200$ MeV and $\mu_b \sim 0.6$ GeV. Phase transition is considered as a first-order transition. The dashed line in Fig. 1 marks the crossover. In this diagram, $\mu_b \sim 1$ GeV and the near-zero temperature correspond to ordinary nuclear matter. With a rise in quark density, i.e., a rise in μ_b, and keeping a low enough temperature, transition occurs to the phase of increasingly compressed nuclear matter (neutron stars).

In the region above the blue curve, the transition occurs to the phase in which colored partons can propagate over large distances, which accounts for nontrivial collective dynamics. In experiments on collisions of ultrarelativistic heavy ions at LHC and the relativistic heavy ion collider (RHIC), this state of matter is investigated at extremely high energy densities and relatively low values of chemical potentials. The typical values of μ_b and T corresponding to heavy-ion head-on collisions in these colliders are shown in Fig. 1 in blue. At higher densities, a phase of colored superconducting quark matter may appear. The quark–gluon plasma in the context of possible extreme states of matter was reviewed by Fortov [33].

2.2 Quark–gluon plasma in heavy ion collisions and in the early Universe

Current cosmological concepts [34] postulate that our Universe came to be after the Big Bang. It evolved through a few epochs corresponding to different states of matter, starting from formally infinitely high densities and temperatures at the instant of Big Bang (Fig. 2). The earliest stage in the evolution of the Universe was the Planck epoch corresponding to times of order $0 < t < 10^{-43}$ s that was dominated by quantum gravity and string effects.

The Planck epoch was followed by the Grand Unification epoch lasting approximately through time 10^{-36} s after the Big Bang, i.e., up to the 'separation' of strong interactions from other fundamental interactions. Thereafter, the inflationary epoch came, which was some 10^{-36} s $< t < 10^{-32}$ s in duration and characterized by an extremely rapid exponential expansion of the Universe. It was followed by the electroweak epoch with a temperature of order 10^{15} K that lasted 10^{-32} s $< t < 10^{-12}$ s and ended after the separation of electroweak interaction into weak and electromagnetic interactions.

In the QGP epoch (10^{-12} s $< t < 10^{-6}$ s), fundamental gravitational and electromagnetic (strong and weak) interactions assumed the present-day form, but matter still had a very high energy density $\varepsilon \sim 1$ GeV fm^{-3} (to compare, typical nuclear matter density, i.e., energy density inside a nucleon, is on the order of 0.13 GeV fm^{-3}) and very high temperature, $T \sim 10^{12}$ K.

According to lattice calculations, such temperatures and energy densities correspond to the deconfinement phase in QCD. In the QGP epoch, the Universe was filled with dense and hot quark–gluon plasma. This epoch ended when the mean particle energy became lower than a critical value corresponding to the confinement–deconfinement phase transition.

The hadron epoch (10^{-6} s $< t <$ 1 s) started when the Universe cooled below this critical value. In this epoch, quarks were confined inside hadrons. Such phase transition is too weakly manifested to be noticed during astronomical observations; this state of matter needs to be studied in the laboratory in order to understand QGP physics. One can say that the creation of such a state of matter in the laboratory is one of the goals of high-energy heavy-ion collision experiments.[2]

Heavy ion collisions in laboratory experiments can be interpreted as a 'small bang' that partly repeats the Big Bang story [35, 36]. The right panel in Fig. 2 illustrates a collision of two nuclei undergoing Lorentz contraction. When these compressed nuclei collide at $t = 0$, their total energy is concentrated within a small volume and its density becomes very high. Quarks and gluons strongly interact immediately after collision, the system heats up, and QGP forms. The time during which the nuclei overlap is estimated as $\tau_{\text{cross}} = 2R/c\gamma$, where γ is the Lorentz factor, and R is the nucleus radius. For RHIC $\gamma_{\text{RHIC}} = 100$, for LHC $\gamma_{\text{LHC}} = 1376$ (which corresponds to the energies of 200 GeV and 2.76 TeV, respec-

[1] The quark chemical potential is a measure of the difference between the number of quarks and antiquarks in a system.

[2] Such energy densities and temperatures may also occur in the central part of dense neutron stars.

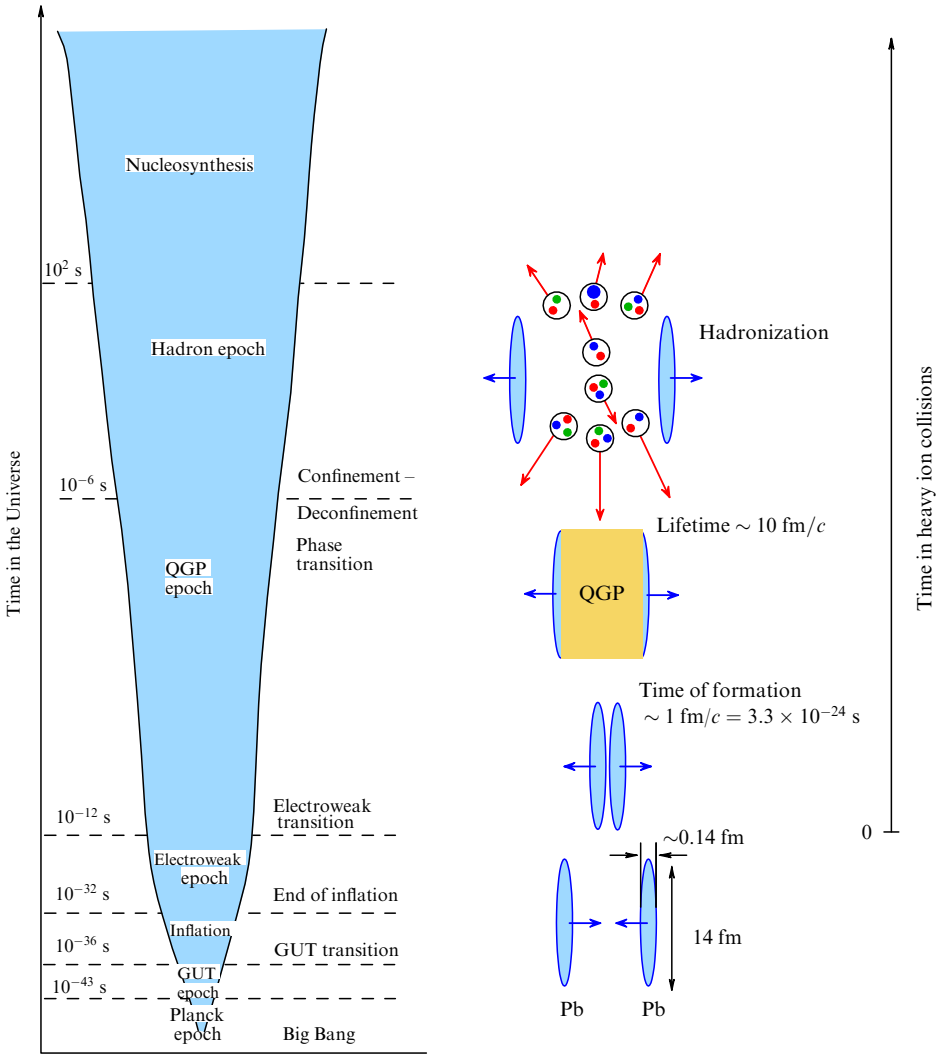

Figure 2. QGP in the early Universe and in heavy ion collisions. GUT — Grand Unification Theory.

tively, i.e., $\tau_{\text{cross}}^{\text{RHIC}} = 0.14$ fm/$c \approx 0.7 \times 10^{-24}$ s, and $\tau_{\text{cross}}^{\text{LHC}} = 0.01$ fm/$c \approx 0.05 \times 10^{-24}$ s); to recall, the characteristic time of strong interactions τ_{strong} is related to QCD characteristic parameter Λ_{QCD}: $\tau_{\text{strong}} \sim 1/\Lambda_{\text{QCD}} \sim 1$ fm/c. The results of measurements of the elliptic flow indicate that after a lapse of 0.2 fm/c matter demonstrates the collective behavior resembling that of a fluid in local equilibrium [1–5] (see also the recent review [15] and references cited therein).

Thereafter, the hot and dense system formed in heavy ion collisions expands and cools as in the evolution of the early Universe; it eventually becomes rarified and undergoes hadronization. An analog of the cosmological epoch of nucleosynthesis in heavy ion collisions is the kinetic cooling stage, during which the hadronic gas passes into the free expansion phase.

3. Physics of heavy ion collisions

In heavy-ion collision experiments, nuclei collide at ultra-relativistic energies in a center-of-mass system. In the alternating gradient synchrotron (AGS), Brookhaven, commissioned in the 1990s, the nucleon–nucleon collision energy was $\sqrt{s_{NN}} = 4.75$ GeV. It was $\sqrt{s_{NN}} = 17.2$ GeV in the super proton synchrotron (SPS), CERN, $\sqrt{s_{NN}} = 200$ GeV in RHIC, Brookhaven, and $\sqrt{s_{NN}} = 2.76$ TeV in LHC.

Gold ions collided in RHIC, and lead ions in LHC. In 2011, A Toroidal LHC ApparatuS (ATLAS) detector recorded luminosity of 158 μb^{-1} for Pb–Pb collisions with the number of events $N_{\text{event}} = (1.03 \pm 0.02) \times 10^9$.

There is convincing experimental evidence that heavy ion collisions in RHIC and LHC give rise to high-temperature bunches of QGP exhibiting collective behavior [1–15]. It can be stated with reference to Feinberg [37] that a 'boiling operator liquid' forms.

QGP properties can be briefly characterized as follows: the occurrence of hydrodynamic behavior, opacity to colored partons (jet and quarkonium quenching), and transparency to photons and weakly interacting particles.

Plasma bunches in LHC were denser, were bigger, and lived longer than those in RHIC. Specifically, their energy density amounted to ≈ 10 GeV fm^{-3} (thrice that in RHIC), volume ≈ 4800 fm^3 (twice that in RHIC), and lifetime around 10 fm/c (20% longer than in RHIC) [38].

A concise description of basic ideas underlying the arrangement of these experiments is presented in Sections 3.1–3.4. See also Refs [13, 30, 31, 39] for more details.

3.1 Experimental validation of local thermal equilibrium

Particle distribution in a system in thermal equilibrium depends only on temperature, chemical potential, and

particle mass. Therefore, local thermal equilibrium can be deduced from an analysis of the relative distribution of different particles [40, 41].

There are a few ways to estimate the temperature of QGP immediately after its formation. One is to measure the wavelengths of photons emitted from widely spaced sources and passing through the medium. Medium temperature is determined by the analysis of exponential dependence of the number of thermal photons on the transverse momentum p_t. According to the calculations [42], the temperature of the medium is around 220 MeV. (See Ref. [43] for more details about energy losses in QGP.)

Another method for determining the temperature of the newly formed QGP falls back on Debye screening of heavy quark pairs. In a hot and dense QGP (in the deconfinement phase), light quarks can screen interaction forces between heavy quark pairs in quarkonium [44]. Notice that the predicted screening is confirmed by lattice calculations in QCD [45–47]. Weakly coupled quarkonium states decay at low enough temperatures, whereas stronger coupled states persist at higher temperatures. This phenomenon can be used as an effective 'thermometer' for measuring the temperature of QGP generated in heavy ion collisions by distinguishing between quarkonium states that can and cannot exist in QGP [48, 49]. RHIC experiments observed suppression pattern of J/ψ [50–52].

Υ-mesons (bound states of the b-quark and its antiparticle $\bar{b}$-quark) have recently been measured at LHC [53]. Pb–Pb collisions were shown to produce many fewer Υ-mesons than pp-collisions. However, theoretical uncertainties as regards the yield of heavy vector mesons do not allow their use as a thermometer.

3.2 Elliptic flow and jet quenching

Central heavy-ion collision pattern in the plane normal to the beam direction is schematically presented in the right panel of Fig. 2. Figure 3 schematically shows scattering in the beam coordinate system during head-on and noncentral collisions.

A primary 'clump' of quarks and gluons formed in noncentral collisions is not symmetric. In a weak quark–gluon interaction, the particles formed in heavy ion collisions fly apart and cannot be expected to retain information about asymmetry of the primary clump. Only strong interactions between the clump particles prevent the loss of asymmetry information, and traces of initial asymmetry can be seen in the flow of particles created in heavy ion collisions. The traces of anisotropy are more apparent at low shear viscosity, because higher viscosity typically promotes the establishment of homogeneity.

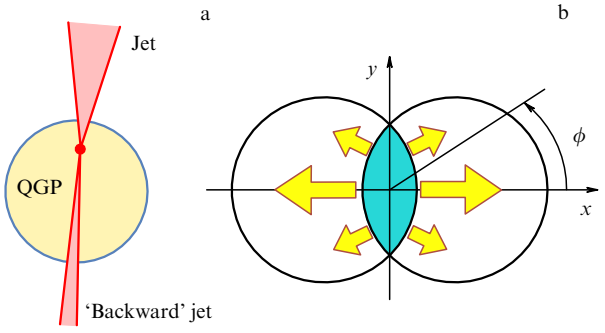

Figure 3. Collisions of two ions in the beam coordinate system. (a) Central collision. (b) Noncentral collision. A droplet of liquid has zero pressure at the edges and high pressure in the middle. Pressure gradients across the 'almond' (parallel to the x-axis) are greater than along it.

Even in head-on ion collisions, the two jets formed in hard collisions at a point localized at a nonzero distance from the center of collision (point A in Fig. 3a) lose energy in different ways. The 'backward' jet loses more energy, because it covers a longer distance in the medium. Figure 3a depicts two such jets propagating in opposite directions in the medium formed in heavy nucleon collisions.

Figure 3b illustrates a noncentral collision in the plane normal to the collision direction. Here, the impact parameter is comparable to the nucleus radius. The two Lorentz-compressed nuclei (two thin 'pancakes') interact only in the shaded almond-like region. Their parts do not interact outside this region. Were the observed hadrons formed in independent nucleon–nucleon collisions within the almond-shaped region, the hadronic final state would be uniformly distributed over the azimuthal angle ϕ (relative to the beam direction), in accordance with the central limiting theorem of the probability theory. In other words, if the particles left the almond-shaped region as a free flow, their final distribution would be unrelated to the shape of this region, i.e., the particles would be distributed isotropically. However, the uniform distribution over the azimuthal angle is in conflict with experimental data. The nonuniform distribution has an event-by-event character. This observation confirms the hypothesis that nucleon collisions lead to the formation of a strongly interacting medium.

The nonaxially symmetric particle distribution in momentum space is characterized by flow anisotropy parameters of nth order, v_n [54]:

$$\frac{dN}{d\phi} = \frac{N}{2\pi}\left\{1 + \sum_n v_n(p_t, b)\cos\left[n(\phi - \Phi_n)\right]\right\}. \qquad (3.1)$$

Here, dN is the total number of particles emitted into the solid angle between ϕ and $\phi + d\phi$, b is the impact parameter, and Φ_n is the azimuthal angle of the reaction plane. The second Fourier coefficient, v_2, called the elliptic flow, dominates in noncentral collisions, while v_n decreases with increasing n.

It is possible to represent the almond-shaped region as a liquid-filled milieu and evaluate the corresponding flows from hydrodynamic equations. It is also possible to relate entropy distribution to multiplicity, $dS/S \sim dN/N$, assuming the liquid to be perfect and neglecting hadronization. In hydrodynamics, the almond-shaped region depicted in Fig. 3b can be represented as a droplet with zero pressure at the edges and high pressure in the center. Pressure gradients are greater across the 'almond' than parallel to it. Therefore, when the droplet bursts, it is an azimuthally asymmetric burst. Parameters of the liquid, such as temperature and shear viscosity, are deduced from the observed v_2 value. According to RHIC experiments [7], the ratio of the viscosity coefficient to entropy density is $\eta/s \approx 0.03-0.15$. This liquid has the lowest viscosity known in nature.

Another consequence of the formation of a hot and dense medium is jet quenching [55–57]. In perturbative QCD, there are well-developed methods based on factorization ideas allowing us to describe jet formation in hard processes associated with high-energy hadron–hadron scattering (see, e.g., reviews [58, 59]). Heavy ion collisions also give rise to jets that are not, however, a mere superposition of the jets formed in pairwise hadron collisions. The jets are

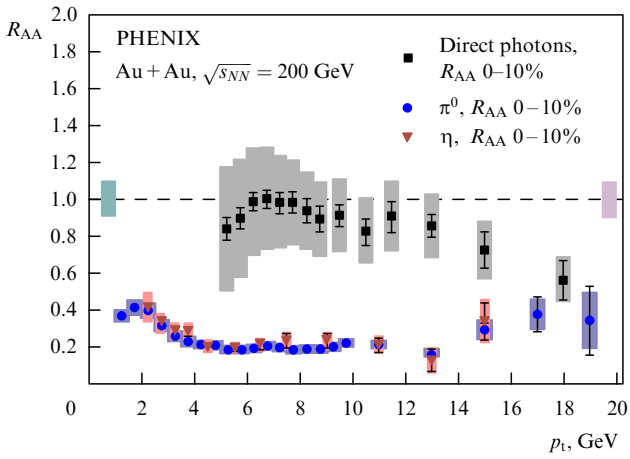

Figure 4. Jet quenching in the PHENIX experiment (Pioneering High Energy Nuclear Interaction eXperiment) at RHIC (preliminary results of the PHENIX collaboration): high-momentum π- and η-mesons are suppressed, unlike colorless neutral photons. (Taken from Ref. [18].)

quenched (suppressed) depending on their direction. Jet quenching is naturally explained on the assumption that the jets pass through the medium interacting with them. In this case, the quark transverse momentum inside the jets is supposed to be much higher than the medium temperature.

The nuclear factor R_{AB}^{h} characterizes the difference between the number of hadrons formed in collisions of nucleus A with nucleus B and the number of hadrons formed in proton–proton collisions:

$$R_{AB}^{h}(p_t, \eta, \text{centrality}) = \frac{dN_{\text{medium}}^{AB\to h}/(dp_t\, d\eta)}{\langle N_{\text{coll}}^{AB}\rangle\, dN_{\text{vacuum}}^{pp\to h}/(dp_t\, d\eta)}\,. \quad (3.2)$$

Here, $\langle N_{\text{coll}}^{AB}\rangle$ is the average number of inelastic nuclear A – B collisions with fixed centrality. Generally speaking, the nuclear factor depends on transverse momentum p_t and pseudorapidity η of the particles, their type h, and impact parameter b.

Figure 4 shows that high-momentum π- and η-mesons are suppressed, and their nuclear factors are roughly one fifth the nuclear factor of colorless neutral photons. This phenomenon can be explained based on the factorization idea in hadron–hadron collisions. The double scattering differential cross section for the hadronic spectrum has the form

$$d\sigma^{h_1 h_2\to h+\text{rest}} \sim \sum_{a,b,c}\int f_{a/h_1}(x_a, Q^2) f_{b/h_2}(x_b, Q^2)\, d\sigma_{ab\to cd} \times D_{c/h}(z)\, d\mu(x_a, x_b, z)\,. \quad (3.3)$$

Here, $f_{a/h}(x, Q^2)$ is the parton distribution function, $\sigma_{ab\to cd}$ is the parton scattering cross section, $D_{c/h}(z_c, Q^2)$ is the fragmentation function whose evolution over Q is defined by the Gribov–Lipatov–Dokshitser–Altarelli–Parisi equation [60–62], z, x_a, x_b are fractions of hadron's momentum h, h_a, h_b carried by the respective partons (in the infinite momentum system), $Q^2 = p_t^2$, and measure $d\mu(z, x_a, x_b)$ takes into account the law of energy and momentum conservation. Hard collisions correspond to large p_t.

Considering a collision between two ions as a mere superposition of a number of pairwise collisions between nucleons, using the data on proton–proton collisions and the estimated characteristics of pairwise nucleon collisions makes it possible to assess the spectrum pattern of the particles produced in heavy ion collisions. In particular, such a scenario suggests that heavy ion collisions must give birth to a large number of high-energy particles, because a part of the particles produced in proton–proton collisions have a rather high energy. However, experimental data indicate that heavy ion collisions result in the suppression of high-energy particles in the final state [1–4]. This observation confirms the occurrence of jet quenching effect in heavy ion collisions.

Thus, we can say that, QGP obtained in RHIC [1, 2] and LHC [5] experiments behaves like a strongly interacting liquid rather than a gas consisting of quarks and gluons [8, 9]. This means that methods of the perturbation theory cannot be applied in describing QGP. QCD lattice methods are equally unsuitable here because they are poorly adapted to the study of real-time processes. Therefore, it seems appropriate to turn to the holographic duality approach for describing QGP [20–22].

3.3 Characteristic times of quark–gluon plasma formation in heavy ion collisions

The collision of two ions results in rapid local thermalization of the parton system followed by its further expansion and cooling, which lead to hadronization and multiparticle production. Experiments have demonstrated a very short thermalization time, $\tau_{\text{therm}} \sim 1$ fm/c, for QGP produced in heavy ion collisions, while cooling time was 20 fm/c [1, 9, 14, 16, 19, 63].

Characteristic times can be described in more detail as follows. 'Hard' processes in a time interval of 0.02 fm/c are responsible for the behavior of 'hard' particles observed in detectors. Semihard processes within time intervals of order 0.2 fm/c are responsible for the main part of 'multiplicity' in the final state. After the thermalization time has elapsed ($\tau_{\text{therm}} \sim 1$ fm/c), the system reaches local equilibrium, called QGP. The further evolution of quark–gluon plasma is described by hydrodynamic equations. After the time period $\tau_{\text{hadr}} \sim 10$ fm/c, the temperature falls below the deconfinement temperature due to bouncing apart of colliding particles and a hot hadronic gas is produced. Further expansion is accompanied by cooling, hadronic gas density becomes low enough by the time of freeze-out, $\tau_f \sim 20$ fm/c, and the system disintegrates into free hadrons observable by detectors.

Thus, heavy-ion collision experiments reveal the following characteristic time hierarchy:

$$\tau_{\text{therm}} < \tau_{\text{hydro}} < \tau_{\text{hadr}} < \tau_f\,. \quad (3.4)$$

Thermalization time τ_{therm} can be roughly estimated from the transverse distribution of energy density ε over rapidity y [64]:

$$\varepsilon(y) = \frac{1}{A\tau_{\text{therm}}}\frac{dN}{dy}\langle m_t\rangle\,, \qquad m_t = \sqrt{m_\pi^2 + k_t^2}\,, \quad (3.5)$$

where m_π is the pion mass, A is the atomic weight, and $\langle m_t\rangle$ is the effective mass derived by averaging over transverse momentum k_t.

Let us discuss the estimate of freeze-out time τ_f. Experimental data suggest the order of τ_f derived from relation [65]

$$\tau_f = R_{\text{long}}\sqrt{\frac{m_t}{T}}\,, \quad (3.6)$$

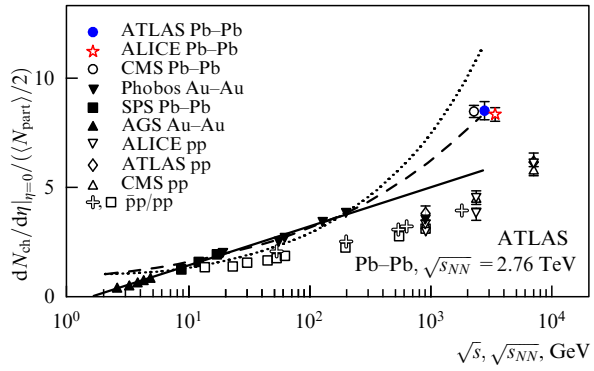

Figure 5. Rapidity density of charged particles per nucleon pair as a function of energy $\sqrt{s_{NN}}$ in nucleus–nucleus collisions and as the function of energy $\sqrt{s}$ in diffraction pp- and p̄p-collisions. Dark dots, stars, white dots, and dark squares are data on Pb–Pb collisions obtained at ATLAS, ALICE, CMS (Compact Muon Solenoid), and SPS, respectively. Dark top-up and top-down triangles are data on Au–Au collisions in the AGS and Phobos experiments. White top-up triangles, diamonds, and top-down triangles are data on pp-collisions from ALICE, ATLAS, and CMS. Crosses and white squares are data from pp- and p̄p-collision experiments. Dotted curve depicts dependence $\sim s_{NN}^{0.25}$ corresponding to Landau's model. Dashed curve shows power-law approximation of ALICE data. Solid line is logarithmic approximation of data obtained in different experiments. (Taken from Ref. [69].)

where T is the freeze-out kinetic temperature assumed to be 0.12 GeV, and $R_{\rm long}$ is the Gaussian longitudinal radius [Hanbury Brown–Twiss (HBT) radius]. The sense of $R_{\rm long}$ becomes clear bearing in mind that $R_{\rm long}$, along with $R_{\rm side}$ and $R_{\rm out}$, describes the spatial pattern of a QGP bunch. In experiments, the expansion rate and spatial extension at the onset of the decoupling regime are measured by the intensity interferometry technique known as HBT analysis and based on the use of the Bose–Einstein correlation between identical boson pairs [66]. This method was successfully employed to study heavy ion collisions in RHIC [67]. The results of LHC measurements of the two-pion Bose–Einstein correlation in central Pb–Pb collisions at an energy of $\sqrt{s_{NN}} = 2.76$ TeV in the center-of-mass system are reported by ALICE Collab. [65]. A rise in energy $\sqrt{s_{NN}}$ was accompanied by the growth not only of $R_{\rm long}$ but also of $R_{\rm side}$ and $R_{\rm out}$. The pion homogeneity region and decoupling regime time exceeded the respective values measured in RHIC. For central Pb-Pb collisions at $\sqrt{s_{NN}} = 2.76$ TeV, the estimate acquired the value of $\tau_{\rm f} \sim 10-11$ fm/c. Hadronization processes in RHIC and LHC are compared in Ref. [68].

3.4 Multiplicity in pp- and AA-collisions

The multiplicity of charged hadrons created in pp and heavy ion collisions rapidly grows with energy in the center-of-mass system. For example, the multiplicity density of charged particles produced in Pb–Pb collisions with an energy of $\sqrt{s_{NN}} = 2.76$ TeV per nucleon pair in A Large Ion Collider Experiment (ALICE) is $dN/d\eta|_{\rm PbPb} = 1584 \pm 4({\rm stat.}) \pm 76({\rm syst.})$ [6]. This value is roughly 1.9 times that in pp-collisions at the same energy, and 2.2 times higher than in central Au–Au collisions at $\sqrt{s_{NN}} = 0.2$ TeV.

Figure 5 compares multiplicity densities of charged particles normalized to the number of involved nucleons, $(dN/d\eta)/(0.5\langle N_{\rm part}\rangle)$, with the results of measurements for Au–Au and Pb–Pb collisions, and pp- and p̄p-collisions for a wide energy region. As noted in Refs [6, 70], the energy dependence plot for heavy nucleon collisions is steeper than for pp- and p̄p-collisions:

$$\left.\frac{dN}{d\eta}\right|_{{\rm PbPb}(s_{NN})} \sim s_{NN}^{0.15}\,, \qquad \frac{\left.(dN/d\eta)\right|_{{\rm PbPb}(s_{NN})}}{\left.(dN/d\eta)\right|_{\rm pp}} = s_{NN}^{0.04}\,. \tag{3.7}$$

4. Relativistic hydrodynamics and quark–gluon plasma

4.1 Landau's hydrodynamic model

The hydrodynamic theory of multiparticle production in ultrarelativistic nuclear particle collisions was elaborated by L Landau in 1953 [25]. Earlier, E Fermi had assumed the possibility of applying statistical methods for the study of this process [26].

Landau postulated the following description of the collision process. The entire process is divided into three stages: (1) the collision proper, (2) the hydrodynamic expansion, and (3) the fly apart. At the first stage, collisions produce a large 'number of particles' concentrated in a region with linear dimensions determined by the radius of action of nuclear forces and the energy of the colliding particles. It is emphasized that the notion of the 'number of particles' in such a system has no exact sense. The particle range in this system is very short compared with its size and must remain small during a certain stage of the expansion process. Therefore, the second stage of the process (expansion) must be of a hydrodynamic nature, the short particle range allowing the matter motion in the system to be considered from the macroscopic (hydrodynamic) standpoint as the motion of an ideal (nonviscous and nonthermoconductive) fluid. Because velocities in the system are comparable with the velocity of light, relativistic hydrodynamic equations should be used. Expansion is followed by the third stage (the fly apart), when the interactions subside, the ranges increase, and the number of particles can be regarded as a physical characteristic.

The total number of particles in the system at the hydrodynamic expansion stage varies. For this reason, the number of particles registered by the detector does not depend on their number produced at the moment of collision but on the number of particles present in the system at the time of transition to the following stage when they fly apart freely [27].

4.1.1 Thermodynamics of fast particle collisions and the total number of particles. The total number of particles produced in collisions depends on their energy and is determined from thermodynamic considerations following from the black body radiation theory. The equation of state for strongly compressed matter in the ultrarelativistic case has the form

$$p = \frac{\varepsilon}{3}\,, \tag{4.1}$$

where p is the pressure, and ε is the energy density. Since the number of particles in the system is not given in advance but depends on statistical equilibrium conditions, the chemical potential is equal to zero: $\mu = \varepsilon - Ts + p = 0$, where s is the entropy per unit volume. Because the first law of thermodynamics for this (unit) volume has the form $d\varepsilon = T\,ds$, the resultant relations are the same as for black body radiation:

$$s \sim \varepsilon^{3/4}\,, \qquad T \sim \varepsilon^{1/4}\,. \tag{4.2}$$

Thereafter, an important assumption is made that the total number N of the newly created particles is proportional to the total entropy of the system: $N = \text{const}\, S$. This gives an opportunity to determine the total number of particles produced in collisions by multiplying entropy density and the volume of a sphere flattened m_A/E times in the longitudinal direction (where E is the energy of each colliding ion in the particles' center-of-inertia system, and m_A is the mass in the rest frame),

$$N = KA^{3/4}\left(\frac{E}{m_{\mathrm{p}}c^2}\right)^{1/2}, \tag{4.3}$$

where K is a constant of order unity, and m_{p} is the proton mass.

4.1.2 Distributions of newly created particles by energies and directions. Let us consider Landau's solution of relativistic hydrodynamic equations describing the angular distribution of newborn particles and their distribution by energies. The relativistic fluid in the Landau model is described by the energy–momentum (stress) tensor $T^{\mu\nu}$ ($\mu, \nu = 0, 1, 2, 3$) of an ideal fluid (A.3) (see Appendix A), the equations have the form (A.1), and the equation of state (4.1) is utilized. It is supposed that matter in the center-of-inertia system takes the form of a disk (initial thickness Δ) strongly flattened in the direction of the $x_\parallel$-axis throughout most of the hydrodynamic expansion stage, and its motion during this time can be regarded as one-dimensional with coordinate $x_\parallel$ and time t:

$$\partial_t T^{00} + \partial_{x_\parallel} T^{01} = 0\,, \qquad \partial_t T^{01} + \partial_{x_\parallel} T^{11} = 0\,, \tag{4.4}$$

where $T^{00} = \varepsilon(u^0)^2 + p(u^1)^2$, $T^{01} = (\varepsilon + p)u^0u^1$, $T^{11} = \varepsilon(u^1)^2 + p(u^0)^2$, and relation $(u^0)^2 - (u^1)^2 = 1$ is fulfilled. At ultrarelativistic velocities, both components, u^0, u^1, are much greater than unity and very similar: $u^0 \approx u^1 = u \gg 1$. In the first approximation, $u^0 - u^1 \approx 1/(2u)$ and hydrodynamic equations (4.4) take the form

$$\partial_t(\varepsilon u^2) = -\frac{1}{4}\,\partial_{x_-}\varepsilon\,, \qquad \partial_t\varepsilon = -\partial_{x_-}\left(\frac{\varepsilon}{u^2}\right). \tag{4.5}$$

Hereinafter, $x_\mp = t \mp x_\parallel$. The approximate solution of Eqns (4.5) in the region $t \gg t_- \gg \Delta$ has the form

$$\varepsilon \sim \exp\left[-\frac{4}{3}\left(a + b - \sqrt{ab}\right)\right], \qquad a = \ln\frac{x_-}{\Delta}\,, \qquad b = \ln\frac{t}{\Delta}\,. \tag{4.6}$$

It can be exploited to find energy and entropy distributions and the formula for the number of newly produced particles per unit solid angle. This consideration holds true at small angles of flight θ.

Remarkably, the two main predictions of Landau's theory, namely the dependence of the ratio of the number of charged particles produced to the number of pairs involved in collisions, $N_{\mathrm{ch}}/(N_{\mathrm{part}}/2)$, on the energy of colliding ions, and the distribution by rapidities are in excellent agreement with experiment in the case of not very high energies. The comparison of distribution by rapidities in the Phobos experiment with Landau distribution is reported in Refs [71–73]. However, Fig. 5 gives evidence that the multiplicity of particles produced at high energies in LHC experiments [6] is in disagreement with predictions of the Landau theory.

Although Landau's hydrodynamics at moderate collision energies fairly well explain multiplicity and rapidity distribution [72, 73], deviations from it at LHC energies [74, 75] require corrections to the Landau approximation and various modifications to the model itself.

If the Landau approximation is not involved, the following equations appear instead of Eqn (4.5) [71, 73]:

$$\begin{aligned} &\frac{\partial\varepsilon}{\partial x_+} + 2\,\frac{\partial\left[\varepsilon\exp\left(-2y_{\mathrm{f}}\right)\right]}{\partial x_-} = 0\,,\\ &2\,\frac{\partial\left[\varepsilon\exp\left(2y_{\mathrm{f}}\right)\right]}{\partial x_+} + \frac{\partial\varepsilon}{\partial x_-} = 0\,. \end{aligned} \tag{4.7}$$

Here, y_{f} is the rapidity of fluid, $u^0 = \cosh y_{\mathrm{f}}$, and $u^1 = \sinh y_{\mathrm{f}}$. Approximate solutions of Eqns (4.7) are discussed in [71, 73, 76–79]. Landau's distribution by rapidities is sensitive to corrections for transverse flows. (See paper [80] for exact solutions with longitudinal and transverse flows in Landau's hydrodynamics.)

It is remarkable that the relativistic hydrodynamics of an ideal fluid provides an adequate description of such important quark–gluon plasma properties as multiplicity and radial and elliptic flows [81–86].

4.2 Kinematics of the Bjorken boost-invariant flow

Boost-invariant dynamics [87] describe quark–gluon plasma expansion under the additional assumption that the physics remain the same in all reference frames moving with a constant velocity along the longitudinal axis. This symmetry can be made explicit by introducing (via relations $t = \tau\cosh y$, $x^\parallel = \tau\sinh y$) the proper time τ and spacetime rapidity y coordinates related to the coordinates in the laboratory frame of reference, time x^0, and position $x^\parallel$ along the expansion axis. In these coordinates, the Minkowski metric takes the form

$$\mathrm{d}s^2 = -\mathrm{d}\tau^2 + \tau^2\,\mathrm{d}y^2 + \mathrm{d}x_\perp^2\,. \tag{4.8}$$

Assume, for simplicity, the presence of symmetry with respect to reflections $y \to -y$, as well as translational and rotational symmetries in the transverse plane. Then, the stress tensor has only three nonzero components: $T_{\tau\tau}$, T_{yy}, and $T_{x_2x_2} = T_{x_3x_3} \equiv T_{xx}$, depending on τ alone. The assumption of conformal invariance for $T_{\mu\nu}$ leads to the tracelessness condition

$$-T_{\tau\tau} + \frac{1}{\tau^2}\,T_{yy} + 2T_{xx} = 0\,. \tag{4.9}$$

Equations of the conservation laws, $D_\nu T^{\mu\nu} = 0$, give the following relationship between the tensor components:

$$\tau\,\frac{\mathrm{d}}{\mathrm{d}\tau}\,T_{\tau\tau} + T_{\tau\tau} + \frac{1}{\tau^2}\,T_{yy} = 0\,. \tag{4.10}$$

The use of equations (4.9) and (4.10) permits expressing the diagonal components of the stress tensor through a single function $f(\tau)$:

$$\mathrm{diag}\, T_{\mu\nu} = \left\{\varepsilon(\tau), \tau^2 p_{\mathrm{l}}, p_{\mathrm{t}}, p_{\mathrm{t}}\right\}, \tag{4.11}$$

$$\begin{aligned} &\varepsilon(\tau) = f(\tau)\,, \qquad p_{\mathrm{l}} = -\tau\,\frac{\mathrm{d}f(\tau)}{\mathrm{d}\tau} - f(\tau)\,,\\ &p_{\mathrm{t}} = f(\tau) + \frac{1}{2}\,\tau\,\frac{\mathrm{d}f(\tau)}{\mathrm{d}\tau}\,, \end{aligned} \tag{4.12}$$

where tensor $T_{\mu\nu}$ is written in (τ, y, x_1, x_2) coordinates, and p_t and p_l are transverse and longitudinal pressures, respectively. The form of the stress tensor (4.11) is totally based on kinematics. The model dynamics determines the choice of a concrete $f(\tau)$ function. An ideal fluid or a fluid with nonvanishing viscosity or other transfer coefficients imply a choice of different $f(\tau)$.

For an ideal fluid, the energy–momentum tensor has the form of the right-hand side in expression (A.3) (see Appendix A). Then, for boost-invariant kinematics in coordinates (τ, y, x_1, x_2), one obtains $u^\mu = (1, 0, 0, 0)$. A comparison of Eqns (A.3) and (4.11) shows that function $f(\tau)$ must have the form

$$f(\tau) = \frac{\text{const}}{\tau^{4/3}} . \tag{4.13}$$

The Bjorken model of an ideal fluid [64] is the limiting case of Landau's model (cf. discussion in Ref. [73]). Indeed, expression (4.6) for energy density in the region $y \ll \ln(t/\Delta)$ gives expression (4.13).

Certain authors have considered SO(3)-invariant, as well as boost-invariant hydrodynamics and their perturbations [88–91] without the assumption of an ideal fluid. Deformation of the Bjorken flow [92] that maintains its usual symmetry in the transverse plane but modifies longitudinal boost-invariance so that interpolation between the Bjorken flow at moderate rapidities and glasma type state at high rapidities has recently been discussed in Ref. [93]. Longitudinal pressure for the energy–momentum tensor describing glasma is roughly equal to energy density taken with the opposite sign [94].

4.3 Problems in the theory of relativistic viscous fluid

For more accurate description of quark–gluon plasma, in particular, for the analysis of its dependence on the choice of initial data, the formalism of relativistic hydrodynamics taking into account dissipation, i.e., viscosity and thermal conductivity is required. Derivation of relativistic equations of motion for a viscous and thermoconductive medium poses a well-known problem: if only terms linear in velocity gradients and thermodynamic quantities in the viscous stress tensor are considered, the resulting theory (so-called first-order formalism) [95, 96] leads to emergence of instability and violation of causality (signal propagation with a superlight velocity). The solution to this problem proposed by Israel and Stewart [97–100] takes account of second-order terms in gradients (see also the recent discussion of this problem for conformal viscous relativistic hydrodynamics in Refs [101–103]).

First- and second-order relativistic equations in gradients for a viscous and thermoconductive medium are presented in Appendix A.

Usually, the second-order approximation in gradients is considered, because the first-order relativistic hydrodynamic equations in gradients allow propagation of perturbations with a superlight velocity [104, 105]. Relativistic hydrodynamic equations within the accuracy of second order in gradients for a conformally invariant fluid were derived in Ref. [101] (see also the recent review [106]). Additional terms for a nonconformal fluid with nonzero bulk (second) viscosity were obtained in Ref. [107] (see also Refs [108, 109]). Vorticity fluctuations in heavy ion collisions were considered in Ref. [110]. The choice of dissipative currents in the Israel–Stewart formalism was also discussed [106, 109].

Numerical calculations of heavy-ion collision dynamics in the framework of the Israel–Stewart formalism for $(2+1)$-dimensions were performed in Refs [111–116] under the assumption of boost-invariance in the longitudinal direction. This assumption is fairly well justified for the intermediate rapidity in collisions at high enough energies, in particular, at LHC. Similar calculations in $(2+1)$-dimensions with the use of the equivalent Ottinger–Grmela formalism are reported in Refs [117, 118]. Recently, $(3+1)$-dimensional calculations for a viscous fluid in a broad rapidity range at lower collision energies were performed in Refs [119–121].

QCD is not a conformally invariant theory; therefore, it must include the nonzero second viscosity coefficient ζ proportional to the trace of the stress tensor [113], i.e., conformal anomaly. The influence of second viscosity on elliptic flow was studied in Ref. [122], and the joint effect of first and second viscosities in Refs [123, 124]. It is expected that second viscosity has a peak (probably together with relaxation time) at critical temperature T_c, when the system acquires a large correlation length [125–128].

The importance of taking into account corrections for second-order hydrodynamics in gradients was emphasized. In the expansion up to third order in gradients [129], the numerical difference from the results of the second-order Israel–Stewart theory is negligibly small at the viscosity to entropy ratio η/s of about 0.05 but becomes essential for $\eta/s \gtrsim 0.2$ (see Ref. [130]).

At the early stages of evolution, when the local distribution over momenta has not yet reached equilibrium and is strongly anisotropic due to rapid longitudinal expansion, viscous corrections to the stress tensor exceed the equilibrium part, which leads to negative pressure. Recent publications [131–134] report attempts to describe both early and later stages of the evolution in the framework of a unified approach based on hydrodynamic expansion in the vicinity of the anisotropic distribution. This leads to new equations of motion, including the equation for the degree of anisotropy of the distribution function.

In one-dimensional [131, 135] and $(2+1)$-dimensional [136] cases, such an approach permits reproducing two limiting cases (free streaming and ideal fluid) and yields second-order hydrodynamic equations in gradients, given expansion in the small anisotropy parameter. Interestingly, entropy calculated in such anisotropic hydrodynamics significantly differs from that calculated in the framework of viscous fluid hydrodynamics up to second order in gradients; this is understandable, since anisotropic hydrodynamics in a limiting case describe free streaming, i.e., a regime far beyond the scope of applicability of viscous fluid hydrodynamics of second order in gradients.

4.4 Elliptic flow and fluctuations of initial data

As mentioned in Section 3.3, RHIC and LHC experiments demonstrated that the distribution of particles produced in off-center collisions over the transverse plane differs from the spherically symmetric distribution (see, for instance, reviews [39, 106, 130, 137–141]). This asymmetry caused by the elliptic flow, i.e., nonzero Fourier coefficient v_2 (see Section 3.2), is naturally explained in hydrodynamic terms.

Additional assumptions with the help of exact solutions of nonlinear hydrodynamic equations give an expression for the elliptic flow [142]. Earlier results obtained in Refs [76, 77, 143] were used in Ref. [142].

Notice that viscosity corrections to ideal hydrodynamics models of multiparticle production began to be calculated after the viscosity to entropy ratio η/s had been computed using AdS/CFT duality [144] (see also Refs [106, 145]). In the case of the $\mathcal{N}=4$ supersymmetric Yang–Mills theory, the ratio $\eta/s = 1/4\pi$ was obtained. Recent numerical calculations in hydrodynamics [140] have shown that the viscosity coefficient is rather small. Also, lattice calculations in QCD were made [127, 146–148], but the possibility of applying static lattice calculations to determine dynamic transfer coefficients remains unclear. Numerical calculations and experimental data gave evidence that η/s values fall within the range $0.07 \leqslant \eta/s \leqslant 0.43$ [141].

Results of numerical calculations in hydrodynamics and their comparison with experimental data illustrate the importance of taking account of the fluctuations in the initial geometric configurations [149–153] (see the recent review [106] and references cited therein).

Fluctuations make both even, $v_2, v_4, \ldots$, and odd, $v_3, v_5, \ldots$, harmonics differ from zero. Different v_n depend on η/s and initial data determined by parton dynamics and fluctuations in the initial ion wave functions. Recent numerical calculations in the framework of hydrodynamic models with fluctuating initial data revealed excellent agreement with flow measurements at RHIC and LHC [154].

A number of methods for taking account of initial data fluctuations in hydrodynamics have been proposed. Specifically, fluid energy density and velocity at the instant of thermalization would be given. One of the most popular models is the Glauber Monte Carlo model [138]. A random impact parameter b is introduced for two ions, and the trajectories of all nucleons are assumed to be rectilinear. Results of numerical calculations in this model [113] give evidence that small deviations from an ideal fluid (corrections for viscosity) substantially change the elliptic flow. Another widely employed model of initial states is the Kharzeev–Levin–Nardi Monte Carlo model based on the employment of color glass condensate (CGC). This approach takes into consideration a well-known property of CGC, namely the predominance of the regime with high gluon density and nonlinear coherence at small values of Bjorken parameter x [155]. High gluon densities correspond to strong classical fields, which permits calculating the wave function from classical field theory equations [11]. One more model makes use of the high-energy wave function consistent with the classical Yang–Mills dynamics of glasma fields [156] induced in heavy ion collisions [157, 158]. This model takes account of the nonlinear nonequilibrium evolution of initial gluon fields.

4.5 Chemical potential

In the case of a nonvanishing chemical potential μ, one has

$$\varepsilon = -p + Ts + \mu n\,, \qquad \mathrm{d}\varepsilon = T\,\mathrm{d}s + \mu\,\mathrm{d}n\,; \tag{4.14}$$

here, $n = N/V$ is the particle number density in volume V. This case suggests the use of equation of state (4.1) and the assumption concerning the relationship between μ and ε. The author of Ref. [159] proposed the relation

$$\mu = \frac{a}{1+\varepsilon/b}\,, \tag{4.15}$$

where $a \approx 1.27$ GeV, and $b \approx 4.3$ GeV. The choice of such a relation is motivated by fitting to experimental data [159] (see also Refs [160, 161]).

Certainly, it would be desirable to obtain the form of energy dependence of the chemical potential by lattice calculations. Such calculations made for a zero chemical potential are sufficient for LHC experiments at the upper energy limit and in the range of intermediate rapidities. Outside this range and at intermediate energies, baryon density becomes essential. The difficulties of lattice calculations for a nonvanishing chemical potential are related to the so-called sign problem arising in the Monte Carlo method applied to fermions. In the case of a small enough baryon chemical potential μ_b, consideration may be confined to the first terms of expansion in μ_b [162], as was reported recently in Ref. [163] using lattice calculations of the first terms of expansion [164, 165].

5. Approach to quark–gluon plasma in the framework of AdS/CFT duality

AdS/CFT duality or gravity/gauge theory duality [20–22] establishes the correspondence between supergravity in 5-dimensional AdS space (approximation to type IIB superstring theory) and conformally invariant gauge theory in the 4-dimensional Minkowski space. Correlation functions of the 4-dimensional gauge theory are expressed in terms of the quantities of 5-dimensional supergravity. A known example of such correspondence is the $\mathcal{N}=4$ supersymmetric Yang–Mills theory — a superconformal theory with matter fields in the adjoint representation of the $\mathrm{SU}(N_\mathrm{c})$ gauge group that is dual to the type IIB superstring theory in $\mathrm{AdS}_5 \times \mathrm{S}^5$ space.

However, a gravity theory dual to QCD is thus far unknown. The difference between the $\mathcal{N}=4$ supersymmetric Yang–Mills theory and QCD becomes less essential when quarks and gluons reside in the deconfinement phase, because due to conformal symmetry the quantum $\mathcal{N}=4$ supersymmetric Yang–Mills theory does not possess confinement. Lattice calculations [166] demonstrate that QCD becomes quasiconformal at a temperature of $T > 300$ MeV and the equation of state can be taken in the form $\varepsilon = 3p$ (the traceless conformally invariant energy–momentum tensor). These considerations prompted the use of AdS/CFT duality for the study of QCD nonperturbative dynamics at high temperatures.

Considerable progress has been achieved in the description of quark–gluon plasma properties, in particular, in the calculation of η/s [144, 167–170] (see also Ref. [171] where violation of the holographic estimation for viscosity is discussed).

In addition, recent calculations in the $\mathcal{N}=4$ supersymmetric Yang–Mills theory indicate that the behavior of collective excitations in the weak coupling regime, calculated by the Keldysh diagram technique [172], does not significantly differ from that in a theory without supersymmetry [173].

Improved holographic models proposed in the last few years incorporate not only gravity but also the lowest string scalar mode — dilaton. The properties of stationary QCD are described using improved holographic models in Section 6.6.

5.1 Correspondence among parameters

Let us consider correspondence between parameters of the gauge theory in the 4-dimensional bulk and the theory in $\mathrm{AdS}_5 \times \mathrm{S}^5$ space.

- The gauge theory has two parameters:

— interaction constant (elementary charge) g;

— number of colors N_c.

The strong and weak coupling limits are defined by 't Hooft parameter $\lambda = g^2 N_c$.

• The string theory has three parameters:

— string length l_s, i.e., characteristic string vibration length;

— string interaction constant g_{st};

— space curvature of additional dimensions R.

These parameters are related by the following expressions [20]:

$$g^2 = 4\pi g_{st}\,, \tag{5.1}$$

$$g^2 N_c = \frac{R^4}{l_s^4}\,. \tag{5.2}$$

In the strong coupling limit in the field theory, one finds $g^2 N_c \gg 1$, and string length is much shorter than the radius of curvature:

$$l_s \ll R\,, \tag{5.3}$$

so that Einstein's gravity can be applied instead of the string theory.

Moreover, the following relationship among G_{10}, g_s, and l_s follows from the string theory (specifically, from the type IIB string theory):

$$16\pi G_{10} = (2\pi)^7 g_{st}^2 l_s^8\,. \tag{5.4}$$

Constant G_{10} is related to the 10-dimensional Planck length: $G_{10} \sim l_P$. Therefore, Eqn (5.4) gives

$$\frac{l_P^8}{l_s^8} \sim g_{st}^2\,. \tag{5.5}$$

It is well-known that classical gravity is applicable if $l_P \ll R$. Whence, one finds

$$\frac{l_P^2}{R^2} = \frac{l_P^2}{l_s^2}\,\frac{l_s^2}{R^2} \sim \sqrt{g_{st}}\,\frac{1}{g\sqrt{N_c}} = \frac{\sqrt{g_{st}}}{\sqrt{4\pi g_{st} N_c}} \sim \frac{1}{\sqrt{N_c}}\,, \tag{5.6}$$

and the Planck length is actually much smaller than the radius of curvature:

$$l_P \ll R\,, \tag{5.7}$$

as $N_c \to \infty$.

5.2 AdS/CFT duality

5.2.1 Euclidean correlation functions in AdS/CFT duality. Let us consider the correspondence between the quantum conformal theory in d-dimensional Euclidean space and classical gravity in AdS_D space, with $D = d + 1$ (see Appendix B). The Euclidean version of AdS_D metric (B.9) has the form

$$ds^2 = \frac{R^2}{z^2}\left(d\tau^2 + d\mathbf{x}^2 + dz^2\right). \tag{5.8}$$

This metric is a solution of the Einstein equations with a negative cosmological constant. In AdS/CFT duality, the d-dimensional quantum field theory is considered at the $\partial M = R^d$ boundary of $M = AdS_D$ space at $z = 0$. Let field ϕ given in the M bulk and acquiring the ϕ_0 value at the boundary ∂M couple to operator $\mathcal{O}$ at the ∂M boundary with interaction Lagrangian $\phi\mathcal{O}$. Then, AdS/CFT duality is formally expressed through the following equality [21, 22]:

$$\left\langle \exp\left(\int_{\partial M} \phi_0 \mathcal{O}\, d^D x\right)\right\rangle = \exp\left\{-S\left[\phi_{cl}(\phi_0)\right]\right\}. \tag{5.9}$$

The left-hand side of Eqn (5.9) contains the generating functional for correlation functions of operator $\mathcal{O}$ in the d-dimensional quantum conformal field theory, while the exponent on the right-hand side of Eqn (5.9) involves action S for the ϕ field evaluated at the classical solution ϕ_{cl} of the equations of motion with the corresponding boundary conditions:

$$\delta S[\phi_{cl}] = 0\,, \qquad \phi_{cl}\Big|_{z=0} = \phi_0\,. \tag{5.10}$$

Formula (5.9) requires renormalization prescription [174, 175].

5.2.2 The scalar field. Let us consider the example of a massless scalar field in Euclidean AdS_D space. The action has the form

$$S = \frac{1}{2}\int_\epsilon^\infty dz \int_{R^d} d\mathbf{x}\; \frac{1}{z^{d-1}} \sum_{i=0}^{d} (\partial_i \phi)^2\,, \qquad \mathbf{x} = (x_1, \ldots, x_d)\,, \tag{5.11}$$

$$x = (x_0, \mathbf{x})\,, \quad x_0 = z\,.$$

Here, $\epsilon > 0$ is the cutoff parameter (see Ref. [21]). Solution of the Dirichlet problem, namely

$$\left(\frac{\partial^2}{\partial z^2} + \sum_{i=1}^{d} \frac{\partial^2}{\partial x_i^2} - \frac{d-1}{z}\,\frac{\partial}{\partial z}\right)\phi = 0\,, \quad \phi\big|_{z=0} = \phi_0(\mathbf{x})\,, \tag{5.12}$$

can be represented in the form

$$\phi(z, \mathbf{x}) = z^{d/2} \int_{R^d} d\mathbf{p} \exp(i\mathbf{p}\mathbf{x})\, |\mathbf{p}|^{d/2} K_{d/2}(|\mathbf{p}|z)\, \tilde{\Phi}_0(\mathbf{p})\,, \tag{5.13}$$

where $K_{d/2}(y)$ is the modified Bessel function, and $\tilde{\Phi}_0$ is a certain arbitrary function. Integration by parts can reduce action (5.11) to the form

$$S = -\frac{1}{2}\int_{R^d} d\mathbf{x}\; \frac{\phi\,\partial_z \phi}{z^{d-1}}\bigg|_{z=\epsilon}\,. \tag{5.14}$$

The asymptotic expansion of the modified Bessel function leads to the renormalized expression for the action. At $d = 4$ in the limit $z \to 0$, it is easy to verify that

$$\phi(z, \mathbf{x}) = C \int_{R^4} d\mathbf{p} \exp(i\mathbf{p}\mathbf{x}) \times \left[2 - \frac{1}{2}(z|\mathbf{p}|)^2 - \frac{(z|\mathbf{p}|)^4}{8} \log\frac{z|\mathbf{p}|}{2} + (z|\mathbf{p}|)^4 + \ldots\right] \tilde{\Phi}_0(\mathbf{p})\,. \tag{5.15}$$

Hereinafter, C, c_1, a, and b are constants, the explicit form of which is unessential.

Action (5.14) has the asymptotics as $\epsilon \to 0$:

$$S = C \int_{R^4} d\mathbf{p}\, |\tilde{\Phi}_0(\mathbf{p})|^2 \left[-\frac{1}{\epsilon^2}|\mathbf{p}|^2 - \frac{|\mathbf{p}|^4}{2} \log\frac{\epsilon|\mathbf{p}|}{2} + c_1|\mathbf{p}|^4 + \ldots\right]. \tag{5.16}$$

The renormalized action is expressed as

$$S_{\rm ren} = \int_{R^4} {\rm d}\mathbf{p}\, |\tilde{\Phi}_0(\mathbf{p})|^2 \left[ap^4 \log|\mathbf{p}|^2 + b|\mathbf{p}|^4\right]. \qquad (5.17)$$

Using the generalized function $|\mathbf{x}-\mathbf{y}|^{-2d}$ [174], action (5.17) at $d=4$ can be represented as

$$S_{\rm ren} = \int_{R^4} \frac{\Phi_0(\mathbf{x})\,\Phi_0(\mathbf{y})}{|\mathbf{x}-\mathbf{y}|^8}\,{\rm d}\mathbf{x}\,{\rm d}\mathbf{y}\,, \qquad (5.18)$$

because the Fourier transform of the generalized function $|\mathbf{x}|^{-8}$ has the form [176, 177]

$$\widetilde{|\mathbf{x}|^{-8}} = ap^4 \log|\mathbf{p}| + b|\mathbf{p}|^4\,.$$

5.2.3 Correlation functions of higher currents and higher-spin fields in AdS space. Relation (5.9) between the field in the M bulk and the conformal operator at the ∂M boundary is generalized to the case of the highest spins, too [23]. Highest spin fields are Fronsdal free fields [178], while conformal operators are conformal currents. In this context, it is interesting to note that the higher spin theory is, in itself, a nontrivial theory posing a number of open questions [179, 180] and allowing the construction of an interacting theory just in AdS space [181]. The duality of the $(\mathcal{N}=4)$-supersymmetric Yang–Mills theory with matter fields in the adjoint representation of the SU($N_{\rm c}$) gauge group and of the type IIB superstring theory in $AdS_5\times S^5$ space naturally includes correspondence between superconformal currents and superstring modes containing all higher spins. Generalization of correspondence (5.9), (5.10) to the case of integer spins is reported in Refs [182, 183]. From the standpoint of applications, an important role is played by the correspondence for spin-2 fields that, in turn, gives a correspondence between the bulk metric and the energy–momentum tensor at the boundary [see relation (5.35) below]. Perhaps classical higher spin fields play a role in the formation of certain stable structures in quark–gluon plasma.

5.2.4 Matsubara thermal correlation functions and BHAdS/TCFT duality. Matsubara correlation functions at a finite temperature (TCFT — Thermal CFT) are calculated using relation (5.9) with the metric of the Euclidean black brane (planar black hole — BHAdS — Black Hole AdS) instead of metric (5.8):

$${\rm d}s^2 = \frac{R^2}{z^2}\left(f(z)\,{\rm d}\tau^2 + {\rm d}\mathbf{x}^2 + \frac{{\rm d}z^2}{f(z)}\right), \qquad (5.19)$$

$$f(z) = 1 - \frac{z^d}{z_{\rm h}^d}\,, \qquad z_{\rm h} = \left(\frac{4\pi T}{d}\right)^{-1}, \qquad (5.20)$$

where $z_{\rm h}$ is the event horizon location, and T is the Hawking temperature. The Euclidean time coordinate τ is assumed to have a period of $1/T$: $\tau\sim\tau+T^{-1}$, and z varies from 0 to $z_{\rm h}$.

5.2.5 AdS/CFT duality in the Minkowski metric. Seemingly, the relationship for AdS/CFT duality in the Minkowski metric would have the form

$$\left\langle \exp\left({\rm i}\int_{\partial{\rm M}} \phi_0 \mathcal{O}\,{\rm d}^D x\right)\right\rangle = \exp\left({\rm i}S_{\rm cl}[\phi]\right). \qquad (5.21)$$

However, such a straightforward analog of the Euclidean version of duality is imperfect [184]. In this version, the classical solution ϕ is uniquely defined by its ϕ_0 value at the $z=0$ boundary, and the requirement of regularity on the horizon: $z=z_{\rm h}$. For this reason, Euclidean correlation functions are uniquely defined by relation (5.9). In the Minkowski metric, the requirement of regularity on the horizon is not sufficient for the uniqueness of the solution. From the standpoint of Green's functions, it is apparent as the existence of many such functions (retarded, advanced, Feynman, etc.) in the field theory. The classical action reduces to the surface term:

$$S = \int \frac{{\rm d}^4k}{(2\pi)^4}\,\phi_0(-k)\,\mathcal{F}(k,z)\,\phi_0(k)\Big|_{z=z_{\rm b}}^{z=z_{\rm h}}, \qquad (5.22)$$

where $z_{\rm b}$ is the position of the boundary, and the acceptable 'recipe' for AdS/CFT duality assumes the form

$$G^{\rm r}(k) = -2\mathcal{F}(k,z)\Big|_{z=z_{\rm b}}, \qquad (5.23)$$

where $G^{\rm r}$ is the retarded Green's function. See Ref. [184] for the definition of $\mathcal{F}$ and a detailed discussion of these problems. The Keldysh propagators [172] were used in Ref. [185] to derive Eqn (5.23).

5.2.6 Geodesic approximation in AdS/CFT duality. It was shown in paper [186] that correlation functions of operators $\mathcal{O}_\Delta(t,x_1,\ldots,x_d)$ with the conformal weight Δ, defined by the path integral, can be calculated at large Δ by summation over the geodesics:

$$\left\langle \mathcal{O}_\Delta(t,x_1,\ldots,x_{d-1})\,\mathcal{O}_\Delta(t',x_1',\ldots,x_{d-1}')\right\rangle = \int \mathcal{D}\mathcal{P}\exp\left({\rm i}\Delta L(\mathcal{P})\right) \approx \sum_{\rm geodesics}\exp\left(-\Delta\mathcal{L}\right). \qquad (5.24)$$

Here, the integral is computed over all paths in AdS space, starting and ending at the boundary points $(t,x_1,\ldots,x_{d-1})$ and $(t',x_1',\ldots,x_{d-1}')$, $L(\mathcal{P})$ is the path length $\mathcal{P}$ that becomes imaginary for space-like paths, and $\mathcal{L}$ is the real geodesic length between the boundary points. Such an approximation holds true if $\Delta\gg 1$.

At $d=2$, one can directly verify if formula (5.24) actually gives the correct result for the conformally invariant equal-time two-point correlation function of the renormalized operator:

$$\left\langle \mathcal{O}_\Delta^{\rm ren}\left(t,-\frac{l}{2}\right)\mathcal{O}_\Delta^{\rm ren}\left(t,\frac{l}{2}\right)\right\rangle = l^{-2\Delta}. \qquad (5.25)$$

Indeed, let us consider metric (5.19) in the Lorentz signature at $d=2$, $f(r)=r^2$, and $R=1$ in (r,t,x), $r=1/z$ coordinates:

$${\rm d}s^2 = -f(r)\,{\rm d}t^2 + \frac{1}{f(r)}\,{\rm d}r^2 + r^2\,{\rm d}x^2\,. \qquad (5.26)$$

Consideration of an equal-time geodesic starting and ending near the AdS boundary, $r=r_{\rm reg}$, at the points located l apart on the x-axis reveals that geodesic length $\mathcal{L}$ is related to l as

$$\mathcal{L} = 2\ln(2r_{\rm reg}) + 2\ln\frac{l}{2}\,, \qquad (5.27)$$

where $r_{\rm reg}$ is the regularized value of coordinate r at the boundary (where $r=\infty$). Geodesic length $\mathcal{L}_{\rm AdS}$ tends to infinity as $r_{\rm reg}\to\infty$, which means that divergence appears near the AdS boundary. Consequently, let us define the renormalized length $\delta\mathcal{L}\equiv\mathcal{L}-2\ln r_{\rm reg}$ by cutting off $r_{\rm reg}$ and removing the divergent part of the geodesic length in the 'pure' AdS space (cf. the action renormalization in Ref. [174]). The renormalized equal-time two-point correlator then takes the form

$$\left\langle \mathcal{O}_{\Delta}^{\rm ren}(t,\mathbf{x})\,\mathcal{O}_{\Delta}^{\rm ren}(t,\mathbf{x}')\right\rangle \sim \exp\left(-\Delta\,\delta\mathcal{L}\right)=\exp\left(-\Delta\ln l^2\right), \tag{5.28}$$

corresponding to expression (5.25).

5.2.7 Geodesic approximation in BHAdS/TCFT duality. Let us consider now the black hole metric in AdS_3 space and show that calculating geodesic lengths permits us to find thermal correlation functions in the conformal field theory. The black hole metric is given by expression (5.26), where

$$f=r^2-1\,. \tag{5.29}$$

Similar to Section 5.2.6, consideration of an equal-time geodesic starting and ending near the AdS boundary, $r=r_{\rm reg}$, at points separated l apart on the x-axis shows that lengths $\mathcal{L}$ and l are related as

$$\mathcal{L}=2\ln(2r_{\rm reg})+2\ln\left(\sinh\frac{l}{2}\right), \tag{5.30}$$

and for the renormalized length one has $\delta\mathcal{L}=2\ln[\sinh(l/2)]$. Expression (5.30) can be interpreted in the conformal field theory as follows. The two-point correlation function of scalar field operator $\mathcal{O}_{h_{\rm L},h_{\rm R}}(z,\bar z)$ with conformal dimensions $(h_{\rm L},h_{\rm R})$ of the left and right modes in the 2-dimensional conformal field theory is found from the conformal invariance condition up to the normalization constant:

$$\left\langle \mathcal{O}_{h_{\rm L},h_{\rm R}}(z_1,\bar z_1)\,\mathcal{O}_{h_{\rm L},h_{\rm R}}(z_2,\bar z_2)\right\rangle=\frac{C_{12}}{(z_1-z_2)^{2h_{\rm L}}(\bar z_1-\bar z_2)^{2h_{\rm R}}}\,. \tag{5.31}$$

The expression for the correlation function at finite temperature T is obtained with the help of conformal mapping $w=\ln z/(2\pi T)$ from the infinite plane to a cylinder with circumference of the base $L=1/T$. Then, correlation function (5.31) takes the form

$$\left\langle \mathcal{O}_{h_{\rm L},h_{\rm R}}(w_1,\bar w_1)\mathcal{O}_{h_{\rm L},h_{\rm R}}(w_2,\bar w_2)\right\rangle =\frac{C_{12}(\pi T)^{2h_{\rm L}}(\pi T)^{2h_{\rm R}}}{\sinh^{2h_{\rm L}}\left[\pi T(w_1-w_2)\right]\sinh^{2h_{\rm R}}\left[\pi T(\bar w_1-\bar w_2)\right]}\,. \tag{5.32}$$

Evidently, if we put $w_1=l/2$, $w_2=-l/2$, and $h_{\rm L}=h_{\rm R}=\Delta/2$, expression (5.32) will coincide with the geometric result $\exp(\Delta\,\delta\mathcal{L})$ at $2\pi T=1$.

5.3 Black holes and AdS/CFT duality for quark–gluon plasma

Applying AdS/CFT duality to describe quark–gluon plasma implies correspondence between phenomenological thermodynamic parameters of the plasma (T, E, P, and μ) and parameters characterizing AdS_5-space deformations. In a dual gravitational description, the source of temperature and entropy is regarded to be due to gravitational horizons. In accordance with Refs [187, 188], the relationship between quark–gluon plasma energy density and black hole temperature in the bulk of AdS has the form $E/L^3=3\pi^3T^4/(16G_5)$, where L is the AdS-space radius, and G_5 is the five-dimensional gravitational constant.

In phenomenological hydrodynamic models [25, 64], the state of quark–gluon plasma is characterized by the energy–momentum tensor $T_{\mu\nu}(x^\rho)$, $\mu,\nu,\rho=0,\ldots,3$. In a dual gravitational description, there is correspondence between the energy–momentum tensor and the metric in AdS_5 asymptotic space. It is convenient to make use of the 5-dimensional Fefferman–Graham metric [189]:

$$\mathrm{d}s^2=L^2\,\frac{g_{\mu\nu}(x^\rho,z)\,\mathrm{d}x^\mu\,\mathrm{d}x^\nu+\mathrm{d}z^2}{z^2}\,. \tag{5.33}$$

The flat Minkowski metric $g_{\mu\nu}=\eta_{\mu\nu}$ defines AdS_5 space in Poincaré coordinates. The conformal boundary of 5-dimensional spacetime (5.33) is $z=0$; as $z\to0$, the following expansion would hold:

$$g_{\mu\nu}(x^\rho,z)=\eta_{\mu\nu}+z^4g_{\mu\nu}^{(4)}(x^\rho)+\ldots\,. \tag{5.34}$$

In this case, AdS/CFT duality leads to a remarkably simple relation

$$g_{\mu\nu}^{(4)}(x^\rho)=\frac{N_{\rm c}^2}{2\pi^2}\left\langle T_{\mu\nu}(x^\rho)\right\rangle \tag{5.35}$$

(see, for instance, reviews [175, 190]).

The black hole metric in the Fefferman–Graham coordinates has the form (5.33) with the following nonvanishing components $g_{\mu\nu}(x^\rho,z)$ (see, e.g., Ref. [191]):

$$g_{00}=-\frac{(1-z^4/z_0^4)^2}{1+z^4/z_0^4}\,,\qquad g_{ii}=1+\frac{z^4}{z_0^4}\,. \tag{5.36}$$

Making coordinate substitution $\tilde z\to z/(1+z^4/z_0^4)^{1/2}$ transforms Eqn (5.33) into the standard static metric of the Schwartzschild AdS black hole:

$$\tilde z^2\,\mathrm{d}s^2=-\left(1-\frac{\tilde z^4}{\tilde z_0^4}\right)\mathrm{d}t^2+\mathrm{d}\mathbf{x}^2+\frac{1}{1-\tilde z^4/\tilde z_0^4}\,\mathrm{d}\tilde z^2\,, \tag{5.37}$$

where $\tilde z_0=z_0/\sqrt{2}$ is the location of the black hole horizon (in what follows, the tilde over z is omitted).

In this case, the expansion of metric (5.34) as $z\to0$ leads to a simple hydrodynamic model with the energy–momentum tensor

$$\langle T_{\mu\nu}\rangle\propto g_{\mu\nu}^{(4)}=\mathrm{diag}\left(\frac{3}{z_0^4},\frac{1}{z_0^4},\frac{1}{z_0^4},\frac{1}{z_0^4}\right). \tag{5.38}$$

The two most effective methods applied to elucidate the properties of quark–gluon plasma in heavy ion collisions make use of energy losses by rare high-energy partons and the spectrum of quarkonium, which are produced in these collisions.

A heavy quark traveling in a strongly interacting quark–gluon plasma is subjected to a decelerating force and, therefore, loses energy. In the simplest case, the quark is regarded as an external moving source with fixed velocity v and is supposed to be in thermal equilibrium with the

medium. This is true if the quark mass is much greater than the typical energy scale of the medium (temperature) and quark motion is considered on a time interval greater than the medium relaxation time scale but smaller than the time for which the quark trajectory notably changes. In this limit, heavy quarks are described by the Wilson line along the quark world line.

In a dual description, the Wilson line is given by the classical string configuration, with one end fixed at the point on the boundary where the quark is located, and the string itself hangs down into the bulk [192, 193]. Let us consider a stationary situation in which the quark travels with a fixed speed for a long time and the shape of the string 'trailing' it does not change with time. For certainty, the quark is assumed to travel in the x_1-direction and the string to be parametrized as $\tau = t, \sigma = z$. Finding the string profile is akin to finding the function $x_1(\tau, \sigma)$ satisfying the string equation of motion. Moreover, the solution must fulfill the boundary condition $x_1(t, z \to 0) = vt$. The stationary solution has the form $x_1(t, z) = vt + \xi(z)$ provided that $\xi(z \to 0) = 0$. The induced metric on the world sheet (WS) is expressed as

$$\mathrm{d}s^2_{\mathrm{WS}} = \frac{R^2}{z^2}\left[-\bigl(f(z) - v^2\bigr)\,\mathrm{d}\tau^2 + \left(\frac{1}{f(z)} + \xi'^2\right)\mathrm{d}\sigma^2 + v\xi'(\mathrm{d}\tau\,\mathrm{d}\sigma + \mathrm{d}\sigma\,\mathrm{d}\tau)\right], \tag{5.39}$$

where $f(z) = 1 - z^4/z_0^4$, as in metric (5.37), and the prime denotes differentiation with respect to z. The Nambu–Goto action for this string takes the form

$$S = \mathcal{T}\int \mathrm{d}z\,\mathcal{L}, \qquad \mathcal{L} = -\frac{R^2}{2\pi\alpha'}\frac{1}{z^2}\sqrt{\frac{f(z) - v^2 + f^2(z)\xi'^2}{f(z)}}\,. \tag{5.40}$$

Here, $\mathcal{T}$ is the total time of quark motion, and α' is the string tension. It is easy to find extremal $\xi(z)$ of this action fulfilling the aforementioned initial conditions:

$$\xi(z) = -\frac{vz_0}{2}\left(\operatorname{artanh}\frac{z}{z_0} - \arctan\frac{z}{z_0}\right). \tag{5.41}$$

According to Refs [192, 193], the momentum lost by a heavy quark traveling through the medium is identical to momentum 'flowing down' the boundary along the string in the horizon direction:

$$\frac{\mathrm{d}p}{\mathrm{d}t} = -\frac{\partial\mathcal{L}}{\partial x_1'}\,. \tag{5.42}$$

For the deceleration coefficient η_D defined by the relation $\mathrm{d}p/\mathrm{d}t = -\eta_D p$, AdS/CFT correspondence gives

$$\eta_D = \frac{\pi\sqrt{\lambda}\,T^2}{2m_{\mathrm{q}}}\,. \tag{5.43}$$

Here, m_{q} is the quark mass, and λ is the interaction constant of the $\mathcal{N} = 4$ supersymmetric gauge theory. Modification of this result for QCD is considered in Section 5.6.

5.4 Boost-invariant geometries

Janik and Peschanski [87] found a solution of the Einstein equations in AdS space with the boundary condition (5.34) that corresponds to the energy–momentum tensor in the boost-invariant form (4.11), (4.12). They imposed the boost-invariance condition, as well as symmetry condition $y \to -y$ and symmetry with respect to translations and turns in the transverse plane, on asymptotic AdS_5 geometry [87]. In the most general form, the metric allowing these symmetries in the Fefferman–Graham coordinates is expressed as

$$\mathrm{d}s^2 = \frac{1}{z^2}\left[-\exp\bigl(a(\tau,z)\bigr)\,\mathrm{d}\tau^2 + \tau^2\exp\bigl(b(\tau,z)\bigr)\,\mathrm{d}y^2 + \exp\bigl(c(\tau,z)\bigr)\,\mathrm{d}x_\perp^2 + \mathrm{d}z^2\right]. \tag{5.44}$$

Expansion of three functions, $a(\tau,z)$, $b(\tau,z)$, and $c(\tau,z)$, at small z must begin from z^4, in accordance with formulas (5.34), (5.35) and (4.11), (4.12). The case of $f(\tau) = e_0/\tau^s$, where e_0 is a certain constant, is considered for $0 < s < 4$ in Ref. [87]. To find the form of solution satisfying $\varepsilon(\tau) = 1/\tau^s$ at large times, solutions of the Einstein equations are searched in the form of power series for metric coefficients:

$$a(\tau,z) = \sum_{n=0} a_n(\tau) z^{4+2n}\,, \tag{5.45}$$

where $a_0(\tau) = -\varepsilon(\tau) = -1/\tau^s$. Then, the leading term of τ asymptotics can be picked up from each $a_n(\tau)$ coefficient, neglecting the other terms. However, it is more convenient to presume self-similarity from the very beginning and introduce a 'dilated' variable $v = z/\tau^{3/4}$ on the assumption that metric coefficients are asymptotically functions of v alone, i.e., $a(z,\tau) = a(v)$ as $\tau \to \infty$, $z \to \infty$, with v being fixed. In this limit, the Einstein equations become ordinary differential equations that can be solved analytically. The relevant procedure was described in Ref. [194]. The result can be formulated as follows:

- for arbitrary s, the solution is singular in the sense that singularity appears in curvature invariants $R_{\mu\nu\rho\gamma}R^{\mu\nu\rho\gamma}$;
- the solution is nonsingular only at $s = 4/3$, in accordance with the Bjorken solution;
- in the latter case, the resulting metric assumes the form

$$\mathrm{d}s^2 = \frac{1}{z^2}\left\{-\frac{\bigl[1 - (e_0/3)(z^4/\tau^{4/3})\bigr]^2}{1 + (e_0/3)(z^4/\tau^{4/3})}\,\mathrm{d}\tau^2 + \left(1 + \frac{e_0}{3}\frac{z^4}{\tau^{4/3}}\right)(\tau^2\,\mathrm{d}y^2 + \mathrm{d}x_\perp^2 + \mathrm{d}z^2)\right\}. \tag{5.46}$$

Solution (5.46) is reminiscent of the black hole in the bulk of AdS, but the horizon location in this case depends on time: $z_0 = \sqrt[4]{3/e_0}\,\tau^{1/3}$. The respective temperature and entropy take the forms $T = \sqrt{2}/\pi z_0$, and $S \propto \tau/z_0^3$. In other words, from the standpoint of the 4-dimensional gauge theory, horizon motion in 5-dimensional AdS space corresponds to plasma cooling. To recall, metric (5.46), unlike (5.37), is not the exact solution of the Einstein equations; in fact, it is an approximate solution only at large times and needs to be modified at small times.

5.5 Chemical potential in quark–gluon plasma and AdS/CFT duality

The Reissner–Nordström charged black hole metric in AdS space has the form

$$\mathrm{d}s^2 = -g(R)\,\mathrm{d}t^2 + g^{-1}(R)\,\mathrm{d}R^2 + R^2\,\mathrm{d}\Omega_{D-2}^2\,, \tag{5.47}$$

$$g(R) = 1 - \frac{2M}{R^2} + \frac{Q^2}{R^4} + \frac{\Lambda}{3}\,R^2\,, \tag{5.48}$$

where Λ is a cosmological constant related to the characteristic length a: $\Lambda/3 \equiv 1/a^2$, M and Q are expressed through the Arnovitt–Deser–Misner mass m and charge σ as $M = 4\pi G_5 m/(3\pi^2)$, $Q^2 = 4\pi G_5 \sigma^2/3$, and the electromagnetic field has only one nonvanishing component

$$A_t = -\frac{\sqrt{3}\,Q}{2R^2} + \Phi\,, \tag{5.49}$$

where $\Phi = \sqrt{3}/2(Q/R_+^2)$, and R_+ is the largest root of the equation $g(R) = 0$.

The thermodynamics of a black hole [195] is described by the free energy of the grand canonical ensemble, $W = TI$. Here, I is the action computed from the solution of equation (5.48) with relation (5.49):

$$I = \frac{\pi\beta}{8G_5 a^2}\left(a^2 R_+^2 + R_+^4 - \frac{Q^2 a^2}{R_+^2}\right), \qquad T = \frac{1}{4\pi}\,g'(R_+)\,, \qquad \mu = \frac{\sqrt{3}\,Q}{2R_+^2}\,, \tag{5.50}$$

where T is the Hawking temperature. The relation with the first law of thermodynamics, $\mathrm{d}\mathcal{E} = T\,\mathrm{d}\mathcal{S} + \mu\,\mathrm{d}\mathcal{Q}$, is established through the identification

$$W = \mathcal{E} - T\mathcal{S} - \Phi\mathcal{Q}\,, \qquad \mathcal{E} = m\,, \qquad \mathcal{S} = \frac{S_h}{4G_5}\,, \qquad \mathcal{Q} = Q\,, \qquad \mu = \Phi\,, \tag{5.51}$$

where S_h is the horizon area. The chemical potential is given by vector-potential asymptotics [196, 197]:

$$\mu = \lim_{r\to\infty} A_t(r)\,. \tag{5.52}$$

The state of quark–gluon plasma is characterized by at least two thermodynamic quantities: temperature and chemical potential. A model of quantum field theory may have the chemical potential for any conserved charge. In AdS/CFT duality, two types of chemical potentials are usually considered: one corresponding to the R-charge, and the other to the baryon number.

The baryon charge occurs only when the theory contains flavor groups in a fundamental representation. Introducing flavors via a D7-brane leads to the appearance of a global flavor $\mathrm{U}(N_f)$-symmetry group containing a $\mathrm{U}(1)_b$ baryonic symmetry subgroup, with a consequent emergence, in turn, of an appropriate chemical potential μ_b for this baryon number [198].

5.6 Improved holographic model of quantum chromodynamics

An improved holographic model of quantum chromodynamics was constructed in Refs [199, 200]. The basic idea of these studies consisted in the following: to develop such a model of scalar field (dilaton) minimally interacting with gravity in a 5-dimensional bulk spacetime, in which radial classical solutions of the scalar field repeat the shape of the QCD β-function upon a change in the scale and, at the same time, fit the results of lattice calculations describing thermodynamic confinement/deconfinement phase transition. The action of the 5-dimensional model has the form

$$S = -M_P^3 N_c^2 \int \mathrm{d}^5x\,\sqrt{g}\left(R - \frac{4}{3}(\partial\Phi)^2 + V(\Phi)\right). \tag{5.53}$$

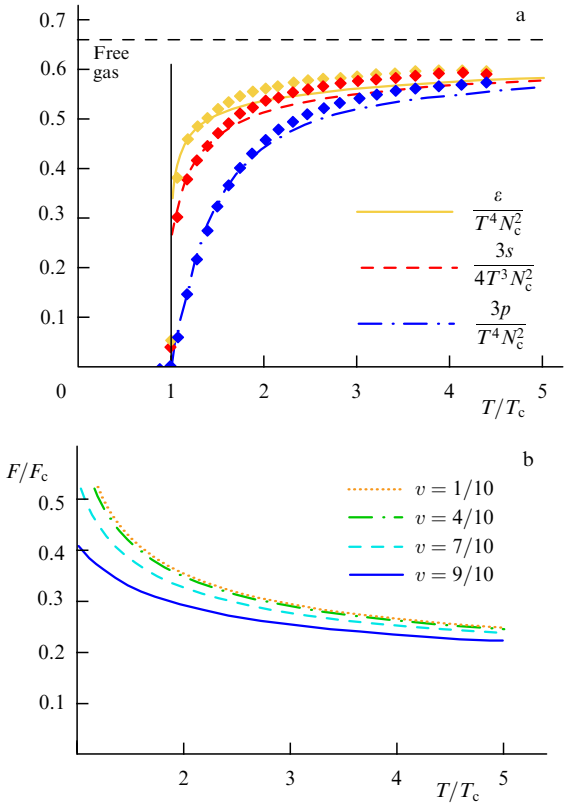

Figure 6. (a) Temperature dependences of energy density ε/T^4 (solid curve), entropy s/T^3 (dashed curve), and pressure p/T^4 (dotted-dashed curve) (critical temperature $T_c = 247$ MeV). Results of lattice calculations at $N_c = 3$ are denoted by diamonds. The curves are obtained by holographic calculations with the use of an improved holographic QCD model (taken from Ref. [93]). (b) Temperature dependence of deceleration forces at different velocities v (taken from Ref. [202]).

Here, M_P is the 5-dimensional Planck mass, g is the determinant of 5-dimensional metric g_{MN}, R is the curvature of this metric, Φ is the dilaton field, and $V(\Phi)$ is its potential. The potential $V(\Phi)$ is searched in such a form that radial solutions for the metric and the field satisfy the relationships

$$\beta(\lambda) \Leftrightarrow 2\,\frac{g_{00}}{g'_{00}}\,\Phi' \exp\Phi\,, \tag{5.54}$$

$$\lambda \Leftrightarrow \exp\Phi\,. \tag{5.55}$$

Here, $\beta(\lambda) = \mathrm{d}\lambda/\mathrm{d}\ln\mu$, g'_{00} is the radial derivative of the metric 00-component. It turned out that the following potential satisfies conditions (5.54), (5.55) [199]:

$$V(\lambda) = \frac{12}{L^2}\left[1 + V_0\lambda + V_1\lambda^{4/3}\sqrt{\log\left(1 + V_2\lambda^{4/3} + V_3\lambda^2\right)}\right], \tag{5.56}$$

where V_2 ensues from the concordance with the β-function at small constants; the best fit to the results of lattice calculations comes about at $V_1 = 14$ and $V_3 = 170$. The temperature dependence of energy density found with the use of an improved holographic QCD model is plotted in Fig. 6a. According to the holographic prescription [201], the glueball spectrum is determined from the effective potential (5.56). The calculated spectrum is compared with the results of lattice calculations in Ref. [202]. Figure 6a displays the temperature dependence of deceleration forces known to be

responsible for energy losses in QGP in accordance with general holographic principles [24].

Notice that correspondences (5.54), (5.55) are in line with the recent proposal [203] to use dimensional reduction of 4-dimensional spacetime ($D = 1 + 3$) to a bulk with a smaller number of spatial dimensions: $D = 1 + d$, $d < 3$, for a rather short-distance analysis of the quantum field theory.

6. Holographic thermalization

6.1 Formation of black holes in AdS space

Spacetime thermalization is defined as the formation of an event horizon (black hole). Let us consider, in particular, the geometries of deformed asymptotically AdS spaces and clarify conditions under which they evolve toward asymptotically AdS spaces with a black hole or black brane (BB). The following picture of possible evolutions of asymptotically AdS bulk geometries emerges.

• The AdS-Schwartzschild space is the equilibrium 'point' in asymptotically AdS bulk geometries (BHAdS point in Fig. 7a).

• Black brane geometry 'points' are the local equilibrium points only with respect to certain 'minor' fluctuations (BBAdS point in Fig. 7a).

• Geometry is stable with respect to minor fluctuations and unstable with respect to relatively large nonlinear fluctuations (AdS point in Fig. 7a).

Hypothetical deformation patterns shown in Fig. 7a are confirmed by numerical calculations. They are altogether different from those in Fig. 7b describing the situation in the Minkowski space. Point M is stable with respect to major fluctuations, because the Minkowski space is stable with respect to finite perturbations [204, 205]. The situation is different in AdS space, which can be unstable with respect to throwing in energy on arbitrarily small scales and simultaneously form small black holes [206–210]. This phenomenon is interpreted as turbulent instability of AdS space. It may be stated that any finite perturbation of AdS space collapses into a black hole after a sufficiently long time.

Small perturbations of black holes/branes in the AdS bulk geometry (deformations near BBAdS and BHAdS points) are studied fairly well. Specifically, quasinormal modes of fields propagating against the black brane background were investigated in Refs [211–216]. These findings were used in the holographic dual approach to QGP for the elucidation of viscosity and other transport coefficients in hydrodynamics (see, for instance, review [217]).

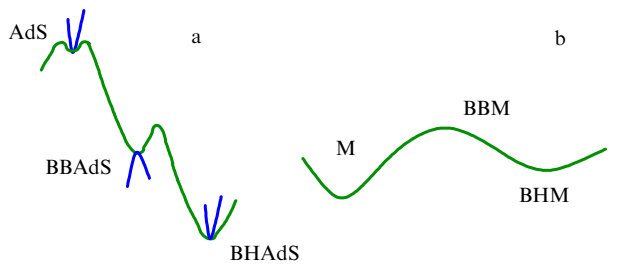

Figure 7. (a) Schematic representation of AdS-space deformations. V-shaped curves near AdS ('empty' AdS space) and BHAdS (black hole in AdS space) points exhibit stability against strain in different directions. Λ-shaped curve near the BHAdS point (black branes in AdS space) suggests instability against strain. (b) Schematic representation of asymptotically Minkowski bulk with a black hole (BHM) and black branes (BBM).

Gravitational collapse of matter thrown in the Minkowski bulk and the formation of an event horizon are traditional problems of interest in GR [218–220]. Naturally, similar problems arise in AdS space.

In the framework of AdS/GFT duality, of special interest are deformations of AdS space dual to alterations of the initial state of the nuclei colliding at ultrarelativistic velocities. In a dual description, such deformations must correspond to the throw-in of matter into the bulk of AdS with a high energy or on very small spatial and temporal scales.

Currently, the following variants of such deformations are considered:

• colliding gravitational shock waves [221–235];

• throw-in of shells of matter with vanishing rest mass ('null dust') [236–249];

• inwardly propagating instantaneous metric perturbations near a boundary [250, 251].

It would be interesting to estimate how long it takes for a black hole to form in AdS space. This issue is of special importance for the study of plasma formation in the holographic dual AdS/CFT description. It was shown in Refs [209, 210] that black holes form very rapidly for the so-called causal boundary time, within a wide range of black hole masses. It is worth mentioning earlier studies of gravitational collapse in AdS_{d+1} space, including estimation of a collapse time (see review [251] and references cited therein). The analog of Chandrasekhar's interpretation of star collapse into a black hole in the AdS/CFT description is considered in Ref. [252]. The formation of a black hole as a result of changing the interaction with matter fields is discussed in Refs [253, 254]. The first two aforementioned cases allow the necessary analytical estimation, even if a partial one. Such calculations are dealt with in Sections 6.2 and 6.3.

6.2 Formation of a black hole in AdS space by a falling shell

In this section, we consider a holographic thermalization model describing black hole formation with the help of Vaidya's metric (more precisely, the AdS-Vaidya metric).

A falling material shell is described by the Vaidya metric

$$\mathrm{d}s^2 = \frac{1}{z^2}\left[-\left(1 - m(v)z^d\right)\mathrm{d}v^2 - 2\,\mathrm{d}z\,\mathrm{d}v + \mathrm{d}\mathbf{x}^2\right], \qquad (6.1)$$

where v is a light-like coordinate, and $\mathbf{x} = (x_1, \ldots, x_{d-1})$ are space-like coordinates at the $z = 0$ boundary. Here, the AdS radius is assumed to be unity. Function $m(v)$ is usually chosen in the form

$$m(v) = M\theta(v), \qquad (6.2)$$

where M is a constant, and $\theta(v)$ is the Heaviside function (Fig. 8).

The change of variables at $m(v) = M$, namely

$$\mathrm{d}v = \mathrm{d}t - \frac{\mathrm{d}z}{1 - Mz^d}, \qquad (6.3)$$

reduces metric (6.1) to the standard form of the black hole metric in Poincaré AdS coordinates:

$$\mathrm{d}s^2 = \frac{1}{z^2}\left[-(1 - Mz^d)\,\mathrm{d}t^2 + \frac{\mathrm{d}z^2}{1 - Mz^d} + \mathrm{d}\mathbf{x}^2\right]. \qquad (6.4)$$

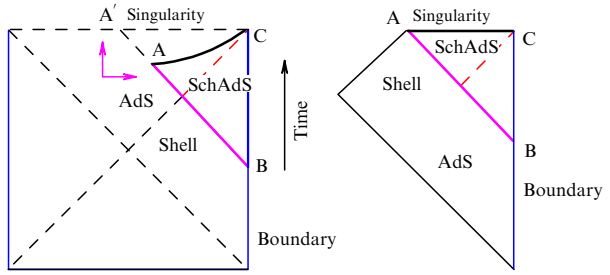

Figure 8. Penrose diagram for the Vaidya-AdS (VAdS) metric (6.1) as a result of the forced gluing of a part of the Penrose diagram for AdS space (see complete Penrose diagram for AdS space in Fig. 14a) and a part of the Penrose diagram for Schwarzschild-AdS (SchAdS) space bounded by the lines connecting points A, B, and C (see complete Penrose diagram for SchAdS in Fig. 14b) along the light-like line AB; point A is glued to point A′ along line AB. Gluing leads to image distortion due to coordinate jumps in the gluing line.

For $v < 0$, metric (6.1), with $m(v)$ in the form (6.2), becomes the AdS space metric.

For metrics (6.1), (6.2) with $d = 2, 3, 4$, geodesics starting and ending at the equal-time points separated l apart on the boundary were studied in Refs [237–241]. In AdS_3 space, the length of the geodesic connecting these points and intersecting the shell is given by the parametric formula

$$\delta\mathcal{L}(t_0, l) = 2\ln\frac{\sinh(r_h t_0)}{r_h\, s(l, t_0)}\,, \tag{6.5}$$

where $s(l, t_0) \in [0, 1]$ is the parameter determined from the condition

$$l = \frac{1}{r_h}\left(\frac{2\varkappa}{s\rho} + \ln\frac{2(1+\varkappa)\,\rho^2 + 2s\rho - \varkappa}{2(1+\varkappa)\,\rho^2 - 2s\rho - \varkappa}\right), \tag{6.6}$$

$$2\rho = \coth(r_h t_0) + \sqrt{\coth^2(r_h t_0) - \frac{2\varkappa}{\varkappa+1}}\,, \tag{6.7}$$

$s = \sqrt{1-\varkappa^2}$, $\rho = 1/(r_h z_c)$, $r_h = \sqrt{M}$, z_c is the position of the 'puncture' in the geodesic shell, and $\varkappa$ is an arbitrary parameter. Clearly, at any l and long enough time, the geodesic connecting boundary points will be wholly inside the black hole; then, the geodesic length will be defined by the expression $\delta\mathcal{L}_{\text{thermal}}(l) = 2\ln(\sinh r_h l/2) - 2\ln r_h$ that coincides with relationship (5.30) at $r_h = 1$, thus implying thermalization for any arbitrary large l. This means that thermalization time in a 2-dimensional bulk equals half the distance between the points. Analysis made in Ref. [244] shows that thermalization time decreases with increasing space dimension.

Freeze-out is described using the AdS-Vaidya metric with a negative energy (negative mass function) [244] (cf. Ref. [255], where black hole evaporation is considered by invoking Hawking radiation). The metric of this process is given by expression (6.1) with $m(v) = M\theta(v) - M_1\theta(v - v_1)$. The case of complete dethermalization corresponds to $M = M_1$. More sophisticated simulations based on the Vaidya shell model in anisotropic deformation of AdS space with black holes/branes [245, 246], i.e., in the space with Lifshitz scaling, are examined in Refs [247, 248]. Thermalization depending on the centrality of collisions is dual to AdS-Vaidya–Kerr shell dynamics [249]. It was revealed for a 2-dimensional case that thermalization time is unrelated to the Kerr parameter.

6.3 Formation of a black hole in shock wave collisions in AdS_5 space

6.3.1 Shock waves in AdS_5 space. Shock waves (SWs) propagating in AdS space have the form [256–261]

$$\mathrm{d}s^2_{\text{SW}} = L^2\,\frac{-\mathrm{d}u\,\mathrm{d}v + \mathrm{d}x_\perp^2 + \phi(x_\perp, z)\delta(u)\,\mathrm{d}u^2 + \mathrm{d}z^2}{z^2}\,. \tag{6.8}$$

Here, u and v are light cone coordinates, and $x_\perp$ is the coordinate normal to the direction of shock wave propagation and the z-axis. This metric corresponds to the energy–momentum tensor T_{MN} with a single nonvanishing component T^{SW}_{uu} given by

$$T^{\text{SW}}_{uu} = J_{uu}(z, x_\perp)\,\delta(u)\,, \tag{6.9}$$

and the Einstein equations reduce to the expression

$$\left(\Box_{H_3} - \frac{3}{L^2}\right)\Phi(z, x_\perp) = -16\pi G_5\,\frac{z}{L}\,J_{uu}(z, x_\perp)\,, \tag{6.10}$$

where the following notation was introduced:

$$\Phi(z, x_\perp) \equiv \frac{L}{z}\,\phi(z, x_\perp)\,, \quad \Box_{H_3} = \frac{z^3}{L^2}\,\frac{\partial}{\partial z}\,\frac{1}{z}\,\frac{\partial}{\partial z} + \frac{z^2}{L^2}\left(\frac{\partial^2}{\partial x_\perp^2}\right).$$

Various forms of shock waves originate from different types of sources $J_{uu}(z, x_\perp)$. The most general form of O(3)-invariant shock waves in AdS space, localized at $u = 0$, corresponds to $\Phi^{\text{O}(3)}(z, x_\perp) = F(q)$, where q is the chordal length:

$$q = \frac{(x_\perp^1)^2 + (x_\perp^2)^2 + (z - z_0)^2}{4zz_0}\,.$$

In this case, the Einstein equations are reduced to an ordinary second-order differential equation

$$\begin{aligned} &q(q+1)F''_{qq} + \frac{3}{2}(1+2q)F'_q - 3F = -16\pi G_5 L^2\rho(q)\,,\\ &\rho(q) = \frac{zJ_{uu}(z, x_\perp)}{L}\,. \end{aligned} \tag{6.11}$$

The profile F^{p} of a point-like shock wave with density $\rho^{\text{p}}(q) = E\delta(q)/(\sqrt{q(1+q)}\,L^3)$ has the form

$$F^{\text{p}} = \frac{2G_5 E}{L}\,\frac{8q^2 + 8q + 1 - 4(2q+1)\sqrt{q(1+q)}}{\sqrt{q(1+q)}}\,. \tag{6.12}$$

The profile of a charged point-like shock wave is described by the sum $F = F^{\text{p}} + F^{Q}$, where F^{p} is given by Eqn (6.12) and F^{Q} is the solution of equation (6.11) with $\rho^{\text{p}Q} = 5Q^2/(24\pi \times 64\,L^5[q(q+1)]^{5/2})$; here, Q is the electric charge. More complicated shock waves in AdS space were addressed in Refs [257–263].

A simpler dual description of colliding ions is provided in the case of wall-on-wall collisions in AdS space [226]. Such walls are called domain walls as well. The Einstein equation for the wall profile has the form [226]

$$\left(\partial_z^2 - \frac{3}{z}\,\partial_z\right)\phi(z) = -16\pi G_5\,\frac{E}{L^2}\,\frac{z_0^3}{L^3}\,\delta(z - z_0)\,. \tag{6.13}$$

The consideration of extended wall type shock waves needs clarification. Specifically, the application of the trapped surface technique requires that the trapped surface be compact. Assume the absence of dependence on the part of coordinates (which reduces the problem to one of a smaller dimension) and find a trapped surface for this small-dimensional problem [226]. Then, the question arises as to whether the small-dimensional trapped surface remains the profile of a multidimensional trapped surface? This question implies the introduction of finite-sized domain walls, i.e., regularization [234], in the consideration. The existence of a multidimensional trapped surface in the collisions between domain walls of a finite size was discussed in Ref. [234], where it is shown for a sufficiently general case that, if a trapped surface exists in the small-dimensional problem, it just as well exists for regularized domain walls. To recall, the problem of wave profile regularization in directions the dependence on which is absent in the chosen approximation also pertains to the consideration of boost-invariant configurations [250, 264].

6.3.2 Multiplicity and trapped surface area in AdS_5 space. Gubser, Pufu, and Yarom [221] proposed the following holographic thermalization picture in heavy ion collisions.

• The dual object describing one of the colliding ions is the shock wave (6.8) propagating in AdS_5 space.

• The dual image of two colliding ions is the sum of two shock waves traveling toward each other, and the metric here has the form

$$\mathrm{d}s^2 = \frac{L^2}{z^2}\left[-\mathrm{d}u\,\mathrm{d}v + \mathrm{d}x_\perp^2 + \phi_1(x_\perp, z)\delta(u)\,\mathrm{d}u^2 + \phi_2(x_\perp, z)\delta(v)\,\mathrm{d}v^2 + \mathrm{d}z^2\right]. \tag{6.14}$$

• The collision of two shock waves in AdS_5 space gives rise (under certain conditions) to a black hole; this phenomenon is interpreted as QGP formation.

The so-called trapped surface (TS) technique known in GR [220, 265] allows detecting BH formation. TS constitutes a surface whose normal geodesics all propagate inward [218], due to which front areas decrease. That the presence of ST in the asymptotically AdS spacetime guarantees black hole formation remains to be proved. However, TS is believed to lie behind the event horizon; moreover, the lower bound of BH entropy S_{AdS} is determined by the TS area A_{trapped}:

$$S_{\mathrm{AdS}} \geqslant S_{\mathrm{trapped}} \equiv \frac{A_{\mathrm{trapped}}}{4G_5}\,. \tag{6.15}$$

These conjectures and estimates have recently been confirmed in numerical experiments [266].

In order to employ the duality relation quantitatively, it is necessary to establish the connection of parameters G_5, L, and E in the 5-dimensional bulk with QGP phenomenological parameters. In accordance with results [221], $L^3/G_5 = 16E/(3\pi^3 T^4) \approx 1.9$. This estimate takes into account that, according to the results of lattice calculations in QCD [32], E/T^4 is a slightly varying quantity: $E/T^4 \approx 11$.

In the case being considered, the relationship for AdS/CFT duality (5.35) between the averaged energy–momentum tensor and deformation of the AdS_5 metric takes the form

$$\langle T_{uu}\rangle = \frac{L^2}{4\pi G_5}\lim_{z\to 0}\frac{1}{z^3}\,\Phi(z, x_\perp)\,\delta(u)\,, \tag{6.16}$$

and is used to fix parameter L. This is possible because the right-hand side of formula (6.16) for the point shock wave Φ^{p} defined by Eqn (6.12) gives the following averaged energy–momentum tensor for the field theory on the boundary:

$$\langle T_{uu}\rangle = \frac{2L^4 E}{\pi\left(L^2 + (x^1)^2 + (x^2)^2\right)^3}\,\delta(u)\,. \tag{6.17}$$

The right-hand side of the last formula coincides with the energy density profile in the Wood–Saxon nuclear potential [267, 268], where L has the sense of transverse nuclear radius: $L \approx 4.3$ fm for Au, and $L \approx 4.4$ fm for Pb.

At RHIC, Au nuclei ($A = 197$) collide at energies $\sqrt{s_{NN}} = 200$ GeV, meaning that each nucleus acquires the energy $E = 100$ GeV per nucleon, i.e., its total energy $E \approx E_{\mathrm{beam}} \approx 19.7$ TeV. At LHC, Pb nuclei ($A = 208$) collide at energies $\sqrt{s_{NN}} = 5.5$ TeV, which means that each nucleus has the total energy $E \approx E_{\mathrm{beam}} \approx 570$ TeV, i.e., 10 times that in RHIC experiments. The estimates of the dimensionless parameter EL for Au–Au collisions in RHIC and Pb–Pb collisions in LHC are [221]

$$EL\big|_{\mathrm{Au-Au},\,\sqrt{s_{NN}}=200\ \mathrm{GeV}} \approx 4.3\times 10^5,$$

$$EL\big|_{\mathrm{Pb-Pb},\,\sqrt{s_{NN}}=5.5\ \mathrm{TeV}} \approx 1.27\times 10^7\,.$$

A somewhat different method to fix L or the characteristic scale of colliding extended waves z_0 was proposed in Ref. [226]. In this approach, radius L is identified with the nucleus size, and z_0 with the saturation scale Q_{s} in the CGC model [11, 155].

Calculations [221, 229] showed that entropy in the high-energy collision limit E increases as $E^{2/3}$:

$$S_{\mathrm{trapped}} \approx \pi\left(\frac{L^3}{G_5}\right)^{1/3}(2EL)^{2/3}\,. \tag{6.18}$$

Consideration of noncentral shock wave collisions in AdS_5 space does not significantly change the dependence $E^{2/3}$. However, there is a critical value of the impact parameter above which TS cannot appear [226], in agreement with predictions [224]. Experimental limitations on the impact parameter value for colliding ions above which QGP cannot form are reported in Ref. [226].

The total multiplicity of S_{QGP} emerges from the analysis of experimental data related to the estimation of multiplicity N_{ch} of newborn charged particles; these quantities are related as $S_{\mathrm{QGP}} \approx 7.5 N_{\mathrm{ch}}$ [269]. The relationship between the total multiplicity S_{QGP} found from the analysis of experimental data and entropy of a black hole formed in AdS_5 proved unsatisfactory [221] because the energy dependence (6.18) is at variance with the experimental dependence (3.7). The discrepancy between S_{trapped} and N_{ch} asymptotics suggests the necessity to modify the holographic model itself.

6.3.3 Estimation of multiplicity in deformed AdS_5 space. The energy dependence of multiplicity simulating the experimental dependence (see Fig. 5) is obtained by considering black hole formation in modified AdS spaces with different b-factors:

$$\mathrm{d}s^2 = b^2(r)\left(\mathrm{d}r^2 + \mathrm{d}x^i\,\mathrm{d}x^i - 2\,\mathrm{d}x^+\,\mathrm{d}x^-\right). \tag{6.19}$$

The possibility of such a modification arises from the introduction of the dilaton field. One such modification is

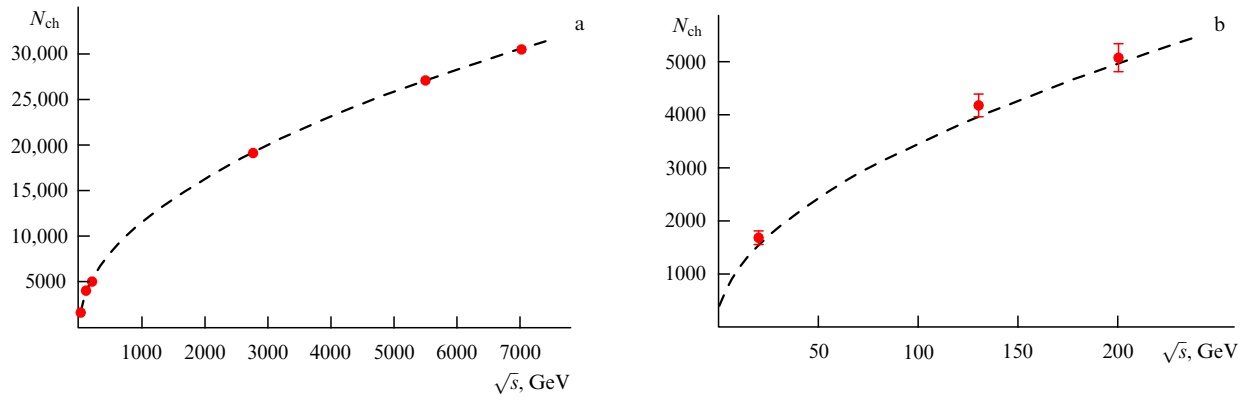

Figure 9. (a) Plot of multiplicity N_{ch} vs energy $\sqrt{s}$. The curve is the result of calculations by formula (6.22), and full dots are RHIC data. (b) Enlarged part of figure (a). (Taken from Ref. [232].)

provided by the dilaton model (5.53) and, in particular, the improved holographic QCD model [199, 200]. The shock wave metric in such models has the form

$$\begin{aligned} ds^2 &= b^2(r)\left(dr^2 + dx^i\,dx^i - 2\,dx^+\,dx^- \right.\\ &\quad \left. + \phi(r, x^1, x^2)\delta(x^+)(dx^+)^2\right), \\ \Phi &= \Phi(r), \end{aligned} \tag{6.20}$$

where $\Phi(r)$ is the scalar field. It is supposed that the metric behaves asymptotically as the AdS metric at $r = 0$. The wave profile satisfies the equation

$$\begin{aligned} &\left(\nabla_\perp^2 + 3\,\frac{b'}{b}\,\partial_r + \partial_r^2\right)\phi = -2\kappa_5^2 J_{++}, \\ &\nabla_\perp^2 \equiv \partial_i\partial_i, \qquad b' \equiv \partial_r b(r), \qquad \kappa_5^2 \equiv 8\pi G_5, \end{aligned} \tag{6.21}$$

with the source J_{++} localized depending on the type of shock wave of interest. It follows from equation (6.21) that the background geometry is determined by the b-factor, the form of which is, in turn, given by the potential in formula (5.53) for the action.

Let us consider a few cases [199, 270, 271] with different IR behaviors of the b-factor ($r \to \infty$ or $r \to r_0$):

• $b \sim r^a$ for $a \leqslant -1$; $a = 1$ corresponds to AdS space. This case, in which the confinement is absent and potential has asymptotics $V \sim \exp(Q\Phi_s)$, $\Phi_s \to \infty$, and $Q < 4/3$, corresponds to the quasiconformal geometry;

• $b(r) \sim (r_0 - r)^a$ for $a > 1/3$ and r_0 determines the position of the IR singularity [271]. The potential in the limit $\Phi_s \to \infty$ has asymptotics $V \sim \exp(Q\Phi_s)$, $Q > 4/3$; moreover, glueballs have a mass gap and a discrete spectrum;

• $b(r) \sim \exp[-(\Lambda r)^a]$ for $a > 0$ describes a situation corresponding to confinement. The potential in the limit $\Phi_s \to \infty$ has asymptotics $V \sim \exp(4\Phi_s/3)\,\Phi_s^{(a-1)/a}$; also, there are a mass gap and a discrete spectrum;

• $b(r) \sim \exp\{-[\Lambda/(r - r_0)]^a\}$ for $a > 0$ and $r_0 > 0$ describes a situation corresponding to confinement. The potential in the limit $\Phi_s \to \infty$ has asymptotics $V \sim \exp(4\Phi_s/3) \times \Phi_s^{(a+1)/a}$.

The problem of black hole formation for modified models in the cases of point-like sources or sources showing a nontrivial dependence on transverse coordinates is sufficiently complicated in itself [232]. Therefore, it would be interesting to invoke domain walls as a model of colliding ions. As shown in Section 6.3.2, such an approach proposed in Ref. [226] requires special regularization at which the finite wall size is introduced [234]. However, the use of domain walls significantly simplifies the problem for modified models and is convenient for the search for models describing the energy dependence of multiplicity close to the experimental one.

The following estimates of TS areas for the aforementioned potentials have been obtained [232, 272]:

• $b \sim r^{-a}$, $a \geqslant 1$. In this case, $A_{trap} \sim s^{(3a-1)/(6a)}$. At $a = 1$, the estimate obtained in Ref. [226] coincides with the estimate for point-like shock waves [221];

• $b(r) \sim (r_0 - r)^a$, $a > 1/3$. At high energies, $A_{trap} \sim s^{n(a)}$, $n(a) = (3a + 1)/(6a)$, and $1/2 < n(a) < 1$;

• $b(r) \sim \exp[-(\Lambda r)^a]$. At high energies, $A_{trap} \sim s^{1/2}(\log s)^{(a+1)/a}$;

• $b(r) \sim \exp\{-[\Lambda/(r - r_0)]^a\}$. At high energies, $A_{trap} \sim s^{1/2}(\log s)^{(1-a)/a}$;

• $b = (L/r)\exp(-r^2/R^2)$. It is this case that corresponds to the improved holographic QCD model [see expression (5.56)].

Taking account of the possible dependence on transverse directions in the last case, the results of numerical calculations [232] lead to the following asymptotics for the multiplicity at high energies:

$$N_{ch} = 78.05\left(\frac{A}{A_{Au}}\,\frac{\sqrt{s}}{1\ \text{GeV}}\right)^{0.451} \log^{0.718}\left(534.9\,\frac{A}{A_{Au}}\,\frac{\sqrt{s}}{1\ \text{GeV}}\right). \tag{6.22}$$

A comparison of the last formula with the RHIC data is presented in Fig. 9.

Importantly, modified models provide better phenomenology in the description of equilibrium QGP properties (see Section 5.6).

6.4 Numerical analysis of shock wave collisions in AdS$_5$ space

To analyze the dynamics of colliding shock waves in the overlap region, the Einstein equations with metric (6.14)-related initial data need to be solved numerically, making use of the smoothed plane waves in the form [87]

$$ds^2 = r^2(-dx_+\,dx_- + d^2x_\perp^2) + \frac{1}{r^2}\left(dr^2 + h(x_\pm)\,dx_\pm^2\right), \tag{6.23}$$

where $x_\pm \equiv t \pm z$, and function h (generally speaking, an arbitrary one) is convenient to choose in the Gaussian form

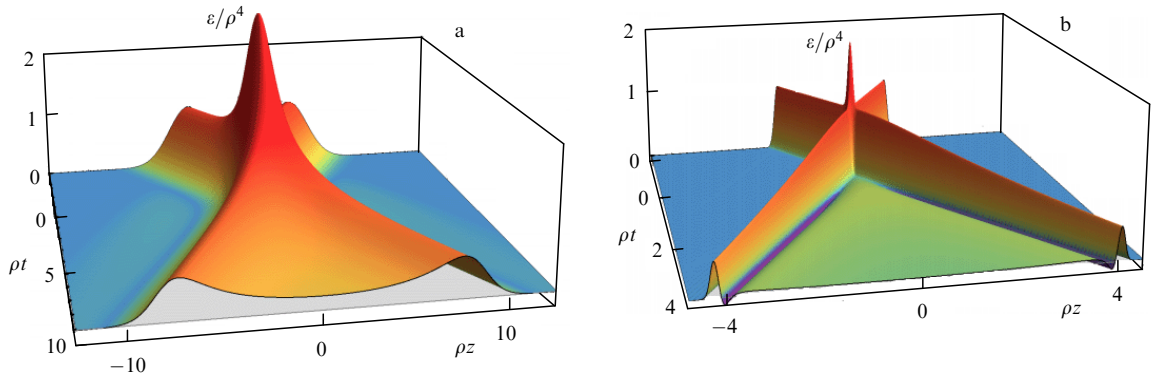

Figure 10. Energy distribution in the holographic picture of shock wave collisions; (a) thick waves, and (b) thin waves. (Taken from Ref. [273].)

with the width w and amplitude μ^3:

$$h(x_\pm) \equiv \mu^3 (2\pi w^2)^{-1/2} \exp\left(-\frac{1}{2}\frac{x_\pm^2}{w^2}\right). \tag{6.24}$$

The energy per shock wave unit area equals $\mu^3(N_c^2/2\pi^2)$. Clearly, if the wave profile has a strongly localized support, the sum of the left and right waves at rather distant time points is the solution to Einstein equations with the respective sources, because each wave is the solution of the Einstein equations with a source. Because Gaussian packets are not localized, sum (6.23) exhibits an approximate solution. The proper initial data are given by taking long enough negative time, on the order of several wave packet widths, and considering the sum of two waves. Upon transforming into Eddington–Finkelstein coordinates, the metric assumes the form

$$\begin{aligned} \mathrm{d}s^2 = &-A\,\mathrm{d}v^2 + \Sigma^2\left[\exp B\,\mathrm{d}^2x_\perp^2 + \exp(-2B)\,\mathrm{d}z^2\right] \\ &+ 2\,\mathrm{d}v\,(\mathrm{d}r + F\,\mathrm{d}z)\,, \end{aligned} \tag{6.25}$$

where A, B, Σ, and F are the functions of r, v, and z. Near the boundary (we consider asymptotically AdS solutions), these functions take the following values:

$$\begin{aligned} &A = r^2\left(1 + \frac{2\xi - 2\partial_v\xi}{r} + \frac{\xi^2 - 2\partial_v\xi}{r^2} + \frac{a_4}{r^4} + O(r^{-5})\right), \\ &F = \partial_z\xi + \frac{f_2}{r^2} + O(r^{-3}), \qquad B = \frac{b_4}{r^4} + O(r^{-5}), \\ &\Sigma = r + \xi + O(r^{-7}), \end{aligned} \tag{6.26}$$

where ξ is the gauge-dependent parameter, and a_4 and f_2 are related to h as

$$a_4 = -\frac{4}{3}\left[h(v_0+z) + h(v_0-z)\right], \quad f_2 = h(v_0+z) - h(v_0-z). \tag{6.27}$$

The numerical analysis made in Ref. [273] has been recently updated in Ref. [273]. The resulting shock wave collision pictures are illustrated in Fig. 10.

Also reported in Ref. [273] is the qualitative difference in the behavior of the energy dependence of colliding waves. Low- and high-energy collisions are simulated as collisions of thick and thin shock waves, respectively. In low-energy collisions, the waves first stop, their original shapes wear off, and further development of waves can be described hydrodynamically. Such a picture is very close to that in the Landau model. At large energies, the colliding waves pass across one another, spread out with the velocity of light, and leave behind regions with negative energy density and longitudinal pressure. The distribution by rapidities is nonboost-invariant. For intermediate rapidities, it is the Gaussian distribution with a width that decreases as energy increases.

7. Gravity/hydrodynamics duality

This section is designed to describe the correspondence between approximate solutions of the Einstein equations in 5-dimensional AdS space and solutions of relativistic hydrodynamic equations with the second-order dissipation in gradients.

7.1 Black brane and ideal fluid

Let us consider Einstein equations

$$R_{MN} - \frac{1}{2}\,g_{MN}R - 6\,g_{MN} = 0\,. \tag{7.1}$$

Here, $M, N = 0, 1, \ldots, 4$, and the units in which $R_{\mathrm{AdS}} = 1$ are chosen. Let us find an approximate solution of these equations for metric g_{MN} such that the metric-based energy–momentum tensor in a 4-dimensional Minkowski bulk satisfies the conservation laws, i.e., relativistic hydrodynamic equations.

Equations (7.1) have solutions of the following form (Eddington–Finkelstein coordinates $r, x^\mu, \mu = 0, 1, 2, 3$ are used):

$$\mathrm{d}s^2 = -2u_\mu\,\mathrm{d}x^\mu\,\mathrm{d}r - r^2 f(br)\,u_\mu u_\nu\,\mathrm{d}x^\mu\,\mathrm{d}x^\nu + r^2 P_{\mu\nu}\,\mathrm{d}x^\mu\,\mathrm{d}x^\nu\,, \tag{7.2}$$

where

$$\begin{aligned} &f(r) = 1 - \frac{1}{r^4}\,, \qquad u^0 = \frac{1}{\sqrt{1-\beta^2}}\,, \\ &u^i = \frac{\beta_i}{\sqrt{1-\beta^2}}\,, \qquad i = 1,2,3, \qquad P^{\mu\nu} = u^\mu u^\nu + \eta^{\mu\nu}\,. \end{aligned} \tag{7.3}$$

Here, b and β_1 are constants, $\beta^2 = \beta_i\beta^i$, and the indices rise and fall with the aid of Minkowski metric: $u_\mu = \eta_{\mu\nu}u^\nu$.

Metric (7.2) describes a black brane with temperature $T = 1/\pi b$ traveling with velocity β_i in the Eddington–Finkelstein coordinates.

Suppose now that b and β_i in metric (7.2) are not constants but slowly changing functions of x^μ coordinates at the AdS boundary: $b(x^\alpha) = T(x^\alpha)/\pi$, $\beta_i(x^\alpha)$; then, the respective metric is written down as

$$\mathrm{d}s^2 = -2u_\mu(x^\alpha)\,\mathrm{d}x^\mu\,\mathrm{d}r - r^2 f\big(b(x^\alpha)r\big)\,u_\mu(x^\alpha)\,u_\nu(x^\alpha)\,\mathrm{d}x^\mu\,\mathrm{d}x^\nu + r^2 P_{\mu\nu}(x^\alpha)\,\mathrm{d}x^\mu\,\mathrm{d}x^\nu\,. \tag{7.4}$$

In general, metric (7.4), denoted below as $g^{(0)}(b(x^\alpha),\beta_i(x^\alpha))$, does not satisfy the Einstein equations. However, the substitution of expression (7.4) into the left-hand side of Einstein equations (7.1) at $M,N=\mu,\nu$ yields the sum of terms, each proportional to the first or second derivatives of $T(x^\alpha)$ or $\beta_i(x^\alpha)$ with respect to x^μ. As a result, this subset of Einstein equations is satisfied up to the first-order gradient terms in x^μ. At the same time, the Einstein equations corresponding to index $M=r$ hold only if functions $T(x^\alpha)$ and $\beta_i(x^\alpha)$ satisfy the equations $\partial_\mu T^{\mu\nu}=0$ for $T^{\mu\nu}=(\pi T)^4(\eta^{\mu\nu}+4u^\mu u^\nu)$. These equations are nothing but relativistic hydrodynamic equations for an ideal fluid with pressure $(\pi T)^4$. This establishes duality between the approximate solution of the Einstein equations and the solution of the relativistic hydrodynamic equations for an ideal fluid.

7.2 Viscosity and gravity

Incorporating a large number of derivatives in the expansion and taking into account the first-order terms in metric derivatives lead to an approximate solution of the Einstein equations up to second-order terms with respect to gradients in the form

$$\begin{aligned}\mathrm{d}s^2 = {}& -2u_\mu\,\mathrm{d}x^\mu\,\mathrm{d}r - r^2 f(br)\,u_\mu u_\nu\,\mathrm{d}x^\mu\,\mathrm{d}x^\nu + r^2\,P_{\mu\nu}\,\mathrm{d}x^\mu\,\mathrm{d}x^\nu \\ & + 2r^2 bF(br)\,\sigma_{\mu\nu}\,\mathrm{d}x^\mu\,\mathrm{d}x^\nu + \frac{2}{3}\,r u_\mu u_\nu\,\partial_\lambda u^\lambda\,\mathrm{d}x^\mu\,\mathrm{d}x^\nu \\ & - r u^\lambda\,\partial_\lambda(u_\nu u_\mu)\,\mathrm{d}x^\mu\,\mathrm{d}x^\nu\,,\end{aligned} \tag{7.5}$$

where

$$F(r) = \frac{1}{4}\left(\ln\frac{(1+r)^2(1+r^2)}{r^4} - 2\arctan r + \pi\right), \tag{7.6}$$

if the equations $\partial_\mu T^{\mu\nu}=0$ are satisfied at $T^{\mu\nu}=(\pi T)^4\times(\eta^{\mu\nu}+4u^\mu u^\nu)-2(\pi T)^3\,\sigma^{\mu\nu}$, with $\sigma^{\mu\nu}=P^{\mu\alpha}P^{\nu\beta}\,\partial_{(\alpha}u_{\beta)}-(1/3)P^{\mu\nu}\,\partial_\alpha u^\alpha$. This energy–momentum tensor describes a fluid with entropy density $s=4\pi^4T^3$ and viscosity $\eta=\pi^3T^3$. Notice that the following relation is valid:

$$\frac{\eta}{s} = \frac{1}{4\pi}\,, \tag{7.7}$$

in agreement with the known result obtained in Ref. [167].

Finally, taking into account the second-order terms in metric derivatives yields an approximate solution of the Einstein equations up to third-order terms if equations $\partial_\mu T^{\mu\nu}=0$ are satisfied. In this case, one finds

$$\begin{aligned}T^{\mu\nu} = {}& (\pi T)^4(\eta^{\mu\nu}+4u^\mu u^\nu) - 2(\pi T)^3\,\sigma^{\mu\nu} \\ & + (\pi T)^2\left[(\ln 2)\,T^{\mu\nu}_{2a} + 2T^{\mu\nu}_{2b} + (2-\ln 2)\left(\frac{1}{3}\,T^{\mu\nu}_{2c} + T^{\mu\nu}_{2d} + T^{\mu\nu}_{2e}\right)\right],\end{aligned} \tag{7.8}$$

where

$$\begin{aligned}T^{\mu\nu}_{2a} &= \epsilon^{\alpha\beta\gamma(\mu}\,\sigma^{\nu)}_{\ \gamma}\,u_\alpha\,\lambda_\beta\,,\\ T^{\mu\nu}_{2b} &= \sigma^{\mu\alpha}\sigma^{\ \nu}_{\alpha} - \frac{1}{3}\,P^{\mu\nu}\,\sigma^{\alpha\beta}\sigma_{\alpha\beta}\,,\\ T^{\mu\nu}_{2c} &= \partial_\alpha u^\alpha \sigma^{\mu\nu}\,,\\ T^{\mu\nu}_{2d} &= Du^\mu Du^\nu - \frac{1}{3}\,P^{\mu\nu}\,Du^\alpha\,Du_\alpha\,,\quad \lambda_\mu = \epsilon_{\alpha\beta\gamma\mu}\,u^\alpha\,\partial^\beta u^\gamma\,,\\ T^{\mu\nu}_{2e} &= P^{\mu\alpha}\,P^{\nu\beta}\,D(\partial_{(\alpha}u_{\beta)}) - \frac{1}{3}\,P^{\mu\nu}P^{\alpha\beta}\,D(\partial_\alpha u_\beta)\,.\end{aligned} \tag{7.9}$$

Here, $\epsilon_{0123}=-\epsilon^{0123}=1$, $D\equiv u^\alpha\partial_\alpha$, and the parentheses enclosing superscripts and subscripts denote symmetrization: $a^{(\alpha}b^{\beta)}=(a^\alpha b^\beta+a^\beta b^\alpha)/2$.

7.3 Conformally invariant fluid and transport coefficients calculated with the use of holography

It is useful to classify all second-order Weyl covariant tensors up to given derivative levels.

Up to the first and second derivative levels there are the following second-order symmetric traceless tensors that transform homogeneously under the Weyl transformation:

$$\begin{aligned}&\text{first level:}\quad \sigma^{\mu\nu};\\ &\text{second level:}\quad \mathfrak{T}^{\mu\nu}_1 = 2u^\alpha\,\mathcal{D}_\alpha\sigma_{\mu\nu}\,,\quad \mathfrak{T}^{\mu\nu}_2 = C_{\mu\alpha\nu\beta}\,u^\alpha u^\beta\,,\\ &\qquad\qquad \mathfrak{T}^{\mu\nu}_3 = 4\sigma^{\alpha\langle\mu}\sigma^{\nu\rangle}_{\ \alpha}\,,\quad \mathfrak{T}^{\mu\nu}_4 = 2\sigma^{\alpha\langle\mu}\omega^{\nu\rangle}_{\ \alpha}\,,\\ &\qquad\qquad \mathfrak{T}^{\mu\nu}_5 = \omega^{\alpha\langle\mu}\omega^{\nu\rangle}_{\ \alpha}\,,\end{aligned}$$

where $\mathcal{D}_\alpha$ is the covariant Weyl derivative introduced in Ref. [274]; here, $\langle^\mu A^{\nu\rangle}$ denotes the symmetric transverse (to vector u) and traceless second-rank tensor built from the ${}^\mu A^\nu$ tensor (by analogy with definition (A.7) in Appendix A). These tensors[3] include velocity derivatives, such as acceleration a^μ and tension $\sigma^{\mu\nu}$. The last two quantities are determined by decomposing the velocity gradient $\nabla^\nu u^\mu$ into the transverse (or traceless) part and the trace:

$$\nabla^\nu u^\mu = -a^\mu u^\nu + \sigma^{\mu\nu} + \omega^{\mu\nu} + \frac{1}{3}\,\theta\,P^{\mu\nu}\,,$$

where divergence, acceleration, and absolute vorticity (rotor) are defined as $\theta=\nabla_\mu u^\mu$, $a^\mu=u^\nu\nabla_\nu u^\mu$, and $\omega^{\nu\mu}=P^{\mu\alpha}P^{\nu\beta}\nabla_{(\alpha}u_{\beta)}$, respectively. Moreover, the 4-dimensional spacetime incorporates vorticity $l^\mu=u_\alpha\,\epsilon^{\alpha\beta\gamma\mu}\nabla_\beta u_\gamma$. Using these notations, gradient corrections to the energy–momentum tensor can be represented in the general form as

$$\begin{aligned}\Pi^{\mu\nu}_{(1)} &= -2\eta\sigma^{\mu\nu}\,,\\ \Pi^{\mu\nu}_{(2)} &= \tau_\Pi\eta\,\mathfrak{T}^{\mu\nu}_1 + \kappa\,\mathfrak{T}^{\mu\nu}_2 + \lambda_1\,\mathfrak{T}^{\mu\nu}_3 + \lambda_2\,\mathfrak{T}^{\mu\nu}_4 + \lambda_3\,\mathfrak{T}^{\mu\nu}_5\,.\end{aligned} \tag{7.10}$$

Thus, there are six transport coefficients: η, τ_Π, κ, λ_i $(i=1,2,3)$, describing a flow of viscous fluid.

Analyzing solutions of gravity equations in AdS_5 space for the holographic description of a fluid makes it possible to find explicit expressions for transport coefficients. Specifi-

[3] A variety of tensor normalization procedures are described in the literature. We choose to use normalization proposed for the first time in Ref. [101]. This accounts for the appearance of factors 2 in the definition of tensors $\mathfrak{T}_i$ (see Ref. [102]).

cally, for the $\mathcal{N}=4$ supersymmetric Yang–Mills theory, the result was obtained as follows[4]

$$\eta=\frac{N^2}{8\pi}\,(\pi T)^3\,,\quad \frac{\eta}{s}=\frac{1}{4\pi}\,,\quad \tau_{\Pi}=\frac{2-\ln 2}{2\pi T}\,,\quad \kappa=\frac{\eta}{\pi\,T}\,,$$
$$\lambda_1=\frac{\eta}{2\pi T}\,,\quad \lambda_2=\frac{\eta\ln 2}{\pi T}\,,\quad \lambda_3=0\,, \tag{7.11}$$

where in the second relation in the first row the known expression for entropy density in the $\mathcal{N}=4$ supersymmetric Yang–Mills theory in the strong coupling regime, $s=\pi^3N^2T^3/2$, is used, giving the known viscosity to the entropy density ratio [144].

Here we presented results for a $d=4$ relativistic fluid dual to the black hole gravitational field in AdS_5 space. These results are generalized to other dimensions, $d\geqslant 3$, in Refs [275, 276].

7.4 Characteristics of thermalization of boost-invariant plasma from holography

Heller et al. [264, 277] considered boost-invariant thermalization of QGP from the holographic point of view. Thermalization of any small perturbations in the bulk of AdS is an exponentially fast process described by quasimodes studied earlier in Ref. [278]. Gravity dual to the expanding plasma is not a stationary solution and looks like a result of the black hole boost. However, thermalization of arbitrarily small perturbation derivatives is equally fast and quasi-exponential, namely $\sim\exp(-\text{const}\,\tau^{2/3})$ [279].

The metric describing a boost-invariant plasma in the Fefferman–Graham coordinates has the form

$$\begin{aligned}\mathrm{d}s^2=\frac{1}{u}\Bigg[&-\left(1-\frac{2\pi^2}{N_c^2}\,\varepsilon(\tau)u^2\right)\mathrm{d}\tau_{FG}^2\\&+\tau_{FG}^2\left(1+\frac{2\pi^2}{N_c^2}\,p_l(\tau)u^2\right)\mathrm{d}y^2\\&+\left(1+\frac{2\pi^2}{N_c^2}\,p_t(\tau)u^2\right)\mathrm{d}x_\perp^2+\frac{1}{4u}\,\mathrm{d}u^2\Bigg]\,.\end{aligned} \tag{7.12}$$

The hydrodynamic equations lead to the following expansion of energy density:

$$\varepsilon(\tau)=\frac{3}{8}\,N_c^2\pi^2\,\frac{\Lambda^4}{(\Lambda\tau)^{4/3}}\left[\varepsilon_2+\frac{\varepsilon_3}{(\Lambda\tau)^{2/3}}+\frac{\varepsilon_4}{(\Lambda\tau)^{4/3}}+\ldots\right], \tag{7.13}$$

where $\varepsilon_2=1$ in the $\mathcal{N}=4$ supersymmetric Yang–Mills theory at large N_c in the strong coupling regime. The single free parameter Λ gives the energy scale. According to formulas (4.11), (4.12), longitudinal and transverse pressures are expressed as

$$p_l=-\varepsilon-\tau\,\frac{\mathrm{d}\varepsilon}{\mathrm{d}\tau}\,,\qquad p_t=\varepsilon+\frac{1}{2}\,\tau\,\frac{\mathrm{d}\varepsilon}{\mathrm{d}\tau}\,. \tag{7.14}$$

Using the notion of effective temperature T_{eff}, relation (7.13) can be presented in the form [170, 280, 281]

$$\varepsilon(\tau)=N_c^2\,\frac{3}{8}\,\pi^2T_{\text{eff}}^4(\tau)\,. \tag{7.15}$$

Temperature T_{eff} is unrelated to real temperature and thermalization; its dependence on $\Lambda\tau$ in the first approximation is expressed as follows:

$$T_{\text{eff}}(\tau)=\frac{\Lambda}{(\Lambda\tau)^{1/3}}\left[1-\frac{1}{6\pi(\Lambda\tau)^{2/3}}+\frac{-1+\log 2}{36\pi^2(\Lambda\tau)^{4/3}}+\frac{-21+2\pi^2+51\log 2-24\log^2 2}{1944\pi^3(\Lambda\tau)^2}+\ldots\right]. \tag{7.16}$$

The expansion of energy density at large τ in powers of $\tau^{-2/3}$ is equivalent to hydrodynamic gradient expansion; it ensues from the expression for velocity gradients ($\nabla_\mu u_\nu\sim\tau^{-1}$) in units of effective temperature.

For a boost-invariant conformal plasma, the conservation laws $\partial_\mu T^{\mu\nu}=0$ can be represented in the form of the first-order differential equation for the scale-invariant quantity $w=T_{\text{eff}}\tau$, namely

$$\frac{\tau}{w}\,\frac{\mathrm{d}w}{\mathrm{d}\tau}=\frac{F_{\text{hydro}}(w)}{w}\,, \tag{7.17}$$

where $F_{\text{hydro}}(w)$ is fully defined in terms of transport coefficients.[5]

For a plasma in the $\mathcal{N}=4$ supersymmetric Yang–Mills theory in the strong coupling regime, there is an explicit form of function $F_{\text{hydro}}(w)/w$ up to third-order hydrodynamic corrections in gradients [281]:

$$\frac{F_{\text{hydro}}^{\text{3rd order}}(w)}{w}=\frac{2}{3}+\frac{1}{9\pi w}+\frac{1-\log 2}{27\pi^2w^2}+\frac{15-2\pi^2-45\log 2+24\log^2 2}{972\pi^3w^3}+\ldots\,. \tag{7.18}$$

Higher-order corrections for energy density (7.13) can be obtained as in Refs [283, 284] by solving the Einstein equations with a negative cosmological constant for the metric taking the form

$$\begin{aligned}\mathrm{d}s^2=&\,2\,\mathrm{d}\tau\,\mathrm{d}r-A\,\mathrm{d}\tau^2+\Sigma^2\exp(-2B)\,\mathrm{d}y^2\\&+\Sigma^2\exp B(\mathrm{d}x_1^2+\mathrm{d}x_2^2)\,,\end{aligned} \tag{7.19}$$

where functions A, Σ, and B depending on r and τ are defined by gradient expansion in accordance with hydrodynamics/gravity duality. A factorial increase in the highest-order gradient expansion has recently been reported [285]. This means that the series of hydrodynamic gradient expansion has a null convergence radius. As is usual in the quantum field theory [286], it is helpful to perform the Borel transform. Reference [285] establishes the equivalence of the leading singularity in the Borel transform to hydrodynamic energy density with lower nonhydrodynamic excitations corresponding to nonhydrodynamic quasinormal gravitational modes. The authors of Refs [282, 287] proposed a conjecture that quasinormal modes can play a role analogous to that of instantons in the context of Borel summation in the quantum field theory [286].

It would be interesting to verify the existence of the universal $F(w)$ function in the right-hand side of Eqn (7.17) with the employment of a numerical solution of the respective gravity equations. In this case (see Section 6.4), the calculation in Fefferman–Graham coordinates poses the singularity problem. It was proposed [264] to solve these gravity

[4] A similar result for the general $\mathcal{N}=1$ superconformal field theory dual to supergravity in $AdS_5\times S^5$ space can be obtained by substituting the respective central charge for quantity $N^2/8\pi^2$ [101, 102].

[5] It resembles the result of Ref. [282] that describes the hydrodynamics taking account of all highest orders of magnitude in terms of linearized AdS dynamics.

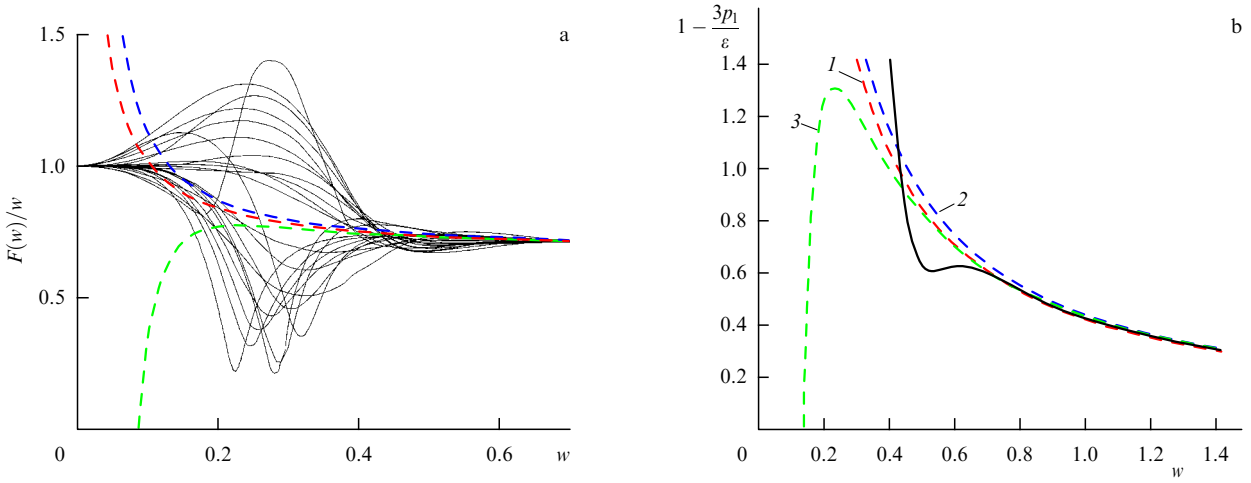

Figure 11. (a) $F(w)/w$ as a function of w for 29 initial data. (b) Pressure anisotropy $1-3p_{\rm l}/\varepsilon$ for the chosen profile. Solid curve is the result of numerical solution of the Einstein equations. Curves *1*, *2*, and *3* correspond to 1st-, 2nd-, and 3rd-order hydrodynamics, respectively. (Taken from Refs [264, 277].)

equations numerically using the Arnovitt–Deser–Misner (ADM) metric in the form [288]

$$\mathrm{d}s^2 = -\frac{a^2(u)\alpha^2(t,u)\,\mathrm{d}t^2}{u} + \frac{t^2a^2(u)b^2(t,u)\,\mathrm{d}y^2}{u} + \frac{c^2(t,u)\,\mathrm{d}x_\perp^2}{u} + \frac{d^2(t,u)\,\mathrm{d}u^2}{4u^2}\,. \tag{7.20}$$

The empty AdS space corresponds to the case in which all coefficient functions equal unity.

Generally speaking, the time coordinate t is not equal to gauge theory proper time τ at the boundary. The relation between AdS time t and proper time τ has the form $\tau \equiv f_0(t) = b(t,0)t/c(t,0)$, while the relations between $\tau_{\rm FG}$ and t, z, and u are expressed as

$$\begin{aligned}\tau_{\rm FG} &= f_0(t) + f_1(t)u + f_2(t)u^2 + \ldots,\\ z &= g_0(t)u^{1/2} + g_1(t)u^{3/2} + g_2(t)u^{5/2} + \ldots.\end{aligned} \tag{7.21}$$

The relationships for $\varepsilon(\tau)$ and $p_{\rm t}(\tau)$ in terms of metric coefficients assume the form

$$\varepsilon(\tau) = \frac{N_{\rm c}^2}{2\pi^2}\,c^4\left(\partial_u^2 a + \frac{2\partial_u a\,\partial_u b}{b} - \partial_u a\,\partial_u d - \frac{\partial_u b\,\partial_u d}{b} - \frac{2\partial_u c\partial_u d}{c} - \frac{9}{4}\,\partial_u d^2 - \frac{\partial_u P}{4tb} - \frac{3M\,\partial_u P}{4c^2} + \frac{\partial_u^2 b}{b} + 2\,\frac{\partial_u^2 c}{c} + \frac{3}{4}\,\partial_u^2 d\right), \tag{7.22}$$

$$p_{\rm t}(\tau) = \frac{N_{\rm c}^2}{2\pi^2}\left(c^3\partial_u^2 c - \frac{1}{4}\,c^4\partial_u d^2 + \frac{1}{4}\,c^4\partial_u^2 d + \frac{1}{4}\,\partial_u d M^2 - \frac{1}{4}\,c^2 M\partial_u P\right). \tag{7.23}$$

Longitudinal pressure $p_{\rm l}(\tau)$ can be found from the tracelessness condition $\varepsilon(\tau) = p_{\rm l}(\tau) + 2p_{\rm t}(\tau)$.

The formation of the hydrodynamic regime starting from configurations far from equilibrium was studied in papers [264, 277]. Despite the emergence of complicated dynamics far off equilibrium, the authors observed correlations between initial and total produced entropies, as well as correlations between the initial temperature and the temperature of transition $T_{\rm hydro-therm}$ to the hydrodynamic description. They also revealed that the hydrodynamics are applicable to a proper time longer than $0.7\,T_{\rm therm}^{-1}$, where $T_{\rm therm}^{-1}$ is the time needed for the isotropic regime to be established.[6]

The numerical solution of the Einstein equations for metric (7.20) using formulas (7.15) and (7.22) was utilized to analyze the quantity $\mathrm{d}\ln w/\mathrm{d}\ln\tau$ for different initial data. In this way, it was shown that function $F_{\rm hydro}(w)/w$ found from equation (7.17) actually exhibits a universal behavior for $w > 0.7$.

To study the transition to hydrodynamics, a numerical criterion for this transition has been introduced. Namely, it was assumed that such a transition is possible if the following condition is fulfilled:

$$\left|\tau\,\frac{\mathrm{d}}{\mathrm{d}\tau}\,\frac{w}{F_{\rm hydro}^{\rm 3rd\ order}(w)} - 1\right| < 0.005\,, \tag{7.24}$$

where the third-order expression is given by formula (7.18).

Strong anisotropy in the energy–momentum tensor during thermalization was revealed [264, 277]. It turned out that the transition to the hydrodynamic description in heavy ion collisions may occur much before isotropization, and a further evolution toward isotropic thermodynamic equilibrium is described in terms of the well-known viscous hydrodynamics.

Figure 11a presents a few curves corresponding to different initial states. Figure 11b shows that nonhydrodynamic modes are important at the initial stage of QGP evolution. There is excellent agreement with hydrodynamics for $w > 0.63$, and high enough anisotropic pressure in this regime is fairly well explained by dissipative hydrodynamics (see Ref. [289] reporting similar observations and some earlier publications [290–293]).

As concerns the entropy, results of numerical calculations suggest the appearance of an apparent horizon (AH),

[6] The authors of Refs [264, 277] refer to the time of transition to the hydrodynamic description as effective thermalization time, and to the isotropization time as true thermalization time. It seems more appropriate to call the time of transition to the hydrodynamic description local thermalization time.

allowing entropy to be defined as the product of $1/4G_N$ and the AH area mapped onto the boundary along the incoming isotropic geodesics [289, 294, 295]. AH entropy density is defined here as the Bekenstein–Hawking entropy density:

$$s_{\rm AH} = \frac{1}{4G_N}\,\frac{t}{u}\,a(u)\,b(t,u)\,c^2(t,u)\Big|_{u=u_{\rm AH}}\,, \tag{7.25}$$

and can be found from the requirement that $\theta_l = 0$, $\theta_n < 0$, where θ_l and θ_n are the expansions [218, 219].

Based on the general considerations of hydrodynamics/gravity duality [294], this entropy can be associated with the boundary entropy that can be obtained by matching horizon and boundary points and using the incoming radial isotropic geodesics [280, 295]. A similar correlation between entropies was also reported for the Vaidya metric [237].

The introduced dimensionless entropy density $s_{n-\rm eq} = 2s_{\rm AH}/(N_{\rm c}^2\pi^2(T_{\rm eff}^{\rm i})^2)$ can be compared with the resulting produced entropy defined at $\tau = \infty$ as $s_{n-\rm eq}^{\rm f} = \Lambda^2(T_{\rm eff}^{\rm i})^{-2}$, where scale Λ is derived from the matching condition for the $T_{\rm eff}$ expression in third-order hydrodynamics [see approximation (7.16)]. Entropy production Δs, defined as the difference $\Delta s = s_{n-\rm eq}^{\rm f} - s_{n-\rm eq}^{\rm i}$, was numerically studied depending on $s_{n-\rm eq}^{\rm i}$ for all examined profiles [277]. Despite a significant difference at the beginning of the evolution, the established dependence of Δs on the initial entropy is accurately described by the formula

$$\Delta s = 1.64(s_{n-\rm eq}^{\rm i})^{1.58}\,. \tag{7.26}$$

Isotropization of the strongly anisotropic original configuration was considered in a later study [269] based on the holographic approach in the framework of the first approximation to the Einstein equation. The Einstein equations were considered in Ref. [269] in the framework of an ansatz of the metric (7.19), making the assumption that the energy–momentum tensor takes the form

$$\langle T_{\mu\nu}\rangle = \frac{N_{\rm c}^2}{2\pi^2}\,{\rm diag}\left[\varepsilon,\, p_{\rm l}(t),\, p_{\rm t}(t),\, p_{\rm t}(t)\right],$$
$$p_{\rm l}(t) = \frac{1}{3}\,\varepsilon - \frac{2}{3}\Delta\mathcal{P}(t)\,, \qquad p_{\rm t}(t) = \frac{1}{3}\,\varepsilon + \frac{1}{3}\,\Delta\mathcal{P}(t)\,,$$

where $\Delta\mathcal{P} = p_{\rm t} - p_{\rm l}$. Such an assumption is different from that made in Ref. [250]. It was shown that to within an accuracy of 10–20%, time $\tau_{\rm iso} \lesssim 1/T$, where T is the finite temperature related to asymptotics $A(r) = r^2 - \pi^4 T^4/r^2 + \ldots$. Stabilization of entropy occurs somewhat earlier. The next orders are considered in recent paper [297]. It is worth mentioning an earlier publication [298], where a radial flow was studied based on the holographic approach.

8. Conclusion

The present review reports the results suggesting that certain observed properties of quark–gluon plasma produced in heavy ion collisions at RHIC and LHC can be described in the framework of the holographic approach based on AdS/CFT duality. The holographic approach permits us to describe energy losses by fast heavy particles, the quarkonium spectrum, QGP transport properties, the multiparticle production phenomenon, small thermalization time, the anisotropic character of local thermalization, and the exit to the hydrodynamic regime.

This new holographic approach poses a number of problems to be addressed in further research, such as extension beyond the Bjorken flow and comprehensive investigations of thermalization processes with the aid of numerical methods in the respective 5-dimensional problem, simulation of shells in deformed AdS space, energy losses by light particles, and the comprehensive inclusion of the chemical potential in the improved AdS/CFT correspondence model.

The holographic approach may be useful to describe high-multiplicity proton–nucleus collisions where according to recent LHC experiments [299–302] the collective behavior is also observed.

The work was supported in part by RFBR grant 11-01-000707-a.

9. Appendices

A. Relativistic equations for a viscous and thermoconductive medium. First and second orders of magnitude in gradients.

A relativistic fluid is described by the energy–momentum tensor $T^{\mu\nu}$, $\mu, \nu = 0, 1, 2, 3$ and a set of currents J_i^μ, $i = 1, 2, \ldots, n$. The equations of motion follow from the conservation laws of the energy–momentum tensor:

$$\partial_\mu T^{\mu\nu} = 0\,, \tag{A.1}$$

and of the corresponding currents

$$\partial_\mu J_i^\mu = 0\,, \tag{A.2}$$

where J_i^μ is the ith conserved current. Neglecting dissipation effects in the case of an ideal fluid leads to the energy–momentum tensor and the currents in the forms

$$T_0^{\mu\nu} = \varepsilon u^\mu u^\nu - p(g^{\mu\nu} - u^\mu u^\nu)\,, \qquad J_{0,\,i}^\mu = n_i u^\mu\,. \tag{A.3}$$

Here, u^μ is the vector field of fluid velocity, $g_{\mu\nu}u^\mu u^\nu = 1$, $g_{\mu\nu}$ is the Minkowski metric, ε is the energy density, p is the pressure, and n_i is the density of the ith conserved charge. Moreover, the equation of state $p = p(\varepsilon, n)$ needs to be given in order to have a closed system of equations.

The expression for $T^{\mu\nu}$ taking account of dissipative effects is written down in the form

$$T^{\mu\nu} = T_0^{\mu\nu} + T_1^{\mu\nu} + T_2^{\mu\nu} + \ldots, \tag{A.4}$$

where tensor $T_1^{\mu\nu}$ contains first-order gradient derivatives of functions u^μ, ε, and p, and tensor $T_2^{\mu\nu}$ contains second-order gradient derivatives of the same functions, etc. The expression for J^μ is constructed by analogy: $J_i^\mu = J_{0,\,i}^\mu + J_{1,\,i}^\mu + \ldots$.

First order in gradients. The velocity vector is defined so that each element of the fluid in the self-frame has zero momentum, and its energy is expressed through other thermodynamic quantities as in the absence of dissipative processes. This condition leads to the relationships (in what follows, consideration is confined to a single current)

$$T_1^{\mu\nu}u^\nu = 0\,, \qquad J_1^\mu u_\mu = 0\,. \tag{A.5}$$

In the first-order approximation in gradients, relativistic equations with dissipation for a fluid assume the form

$$\partial_\mu(T_0^{\mu\nu} + T_1^{\mu\nu}) = 0\,, \qquad \partial_\mu(J_0^\mu + J_1^\mu) = 0\,, \tag{A.6}$$

where

$$T_1^{\mu\nu} = \eta\partial^{\langle\mu}u^{\nu\rangle} - \zeta\partial_\alpha u^\alpha \Delta^{\mu\nu}\,,$$
$$J_1^\mu = \kappa\left(\frac{nT}{w}\right)^2\left[\partial^\mu\left(\frac{\mu_b}{T}\right) - u^\mu u^\nu\partial_\nu\left(\frac{\mu_b}{T}\right)\right].$$

Here, η and ζ are the viscosity coefficients, κ is the thermal conductivity coefficient, T is the temperature, $w = \varepsilon + p$ is the thermal function of unit volume, μ_b is the relativistic chemical potential: $n\mu_b = w - Ts$, where s is the entropy per unit self-volume, and the notation

$$A_{\langle\mu}B_{\nu\rangle} = (\Delta_\mu^\alpha\Delta_\nu^\beta + \Delta_\nu^\alpha\Delta_\mu^\beta - \frac{2}{3}\Delta^{\alpha\beta}\Delta_{\mu\nu})A_\alpha B_\beta \tag{A.7}$$

was introduced, where $\Delta^{\mu\nu} = g^{\mu\nu} - u^\mu u^\nu$ is the projector orthogonal to the velocity vector: $u_\mu\Delta^{\mu\nu} = 0$.

The entropy flux density vector is expressed as

$$s^\alpha = su^\alpha - \frac{\mu_b}{T}J_1^\alpha\,, \tag{A.8}$$

while the law of increasing entropy is given by

$$\partial_\alpha s^\alpha = -J_1^\alpha\partial_\alpha\frac{\mu_b}{T} + \frac{1}{T}T_1^{\mu\nu}\partial_\mu u_\nu\,. \tag{A.9}$$

Second-order Israel–Stewart formalism for a conformal fluid. Second-order hydrodynamic equations in gradients are written down as

$$\partial_\mu(T_0^{\mu\nu} + T_1^{\mu\nu} + T_2^{\mu\nu}) = 0\,. \tag{A.10}$$

The energy–momentum tensor for a conformal fluid [101] in the Israel–Stewart formalism is represented as $\mathcal{T}^{\mu\nu} = T_0^{\mu\nu} + \pi^{\mu\nu}$. The simplest equations of motion assume the form

$$\partial_\mu\mathcal{T}^{\mu\nu} = 0\,,$$
$$\Delta_\alpha^\mu\Delta_\beta^\nu u^\sigma\partial_\sigma\pi^{\alpha\beta} = -\frac{1}{\tau_\Pi}(\pi^{\mu\nu} - T_1^{\mu\nu}) - \frac{4}{3}\pi^{\mu\nu}(\partial_\alpha u^\alpha)\,, \tag{A.11}$$

where τ_Π is a constant (transport coefficient).

Therefore, for a conformal fluid one has $\zeta = 0$, and only the first viscosity coefficient η is conserved. For a conformal viscous fluid, the following expression for second-order corrections in gradients to the energy–momentum tensor was obtained [101, 102]:

$$T_2^{\mu\nu} = -\tau_2\eta\left[\Delta_\alpha^\mu\Delta_\beta^\nu D\sigma^{\alpha\beta} + \frac{4}{3}\sigma^{\mu\nu}(\partial_\alpha u^\alpha)\right] - \lambda_1\sigma_\alpha^{\langle\mu}\sigma^{\nu\rangle\alpha} + \lambda_2\sigma_\alpha^{\langle\mu}\omega^{\nu\rangle\alpha} - \lambda_3\omega_\alpha^{\langle\mu}\omega^{\nu\rangle\alpha}\,. \tag{A.12}$$

Here, $D = u^\alpha\partial_\alpha$, $\nabla^\mu = \Delta^{\mu\nu}\partial_\nu$, $\sigma^{\mu\nu} = \nabla^{\langle\mu}u^{\nu\rangle}$, $\omega_{\mu\nu} = (\nabla_\nu u_\mu - \nabla_\mu u_\nu)/2$, and four additional transport coefficients, τ_2, λ_1, λ_2, and λ_3, appear.

B. AdS_D-space geometry

AdS space is a noncompact manifold of constant curvature with a Lorentzian metric signature. It can be represented as factor-space $\mathrm{AdS}_D = \mathrm{SO}(2,d)/\mathrm{SO}(1,d)$, $D = d+1$. AdS space can be realized as a hyperboloid:

$$\mathrm{AdS}_{d+1} = \left\{X \in \mathrm{R}^{(2;d)}\colon +X_1^2 + \ldots + X_d^2 - X_0^2 - X_{d+1}^2 = -R^2\right\}, \tag{B.1}$$

where $\mathrm{R}^{(2;d)}$ has two time-like dimensions, and d spacetime dimensions. The linear element of anti-de-Sitter space is constructed by restricting the $(D+1)$-dimensional metric onto the AdS_D manifold:

$$\mathrm{d}s^2 = -\mathrm{d}X_{d+1}^2 - \mathrm{d}X_0^2 + \mathrm{d}X_1^2 + \ldots + \mathrm{d}X_d^2\Big|_{\mathrm{AdS}_{d+1}}\,. \tag{B.2}$$

This metric is a maximally symmetric solution of the Einstein equations with a negative cosmological constant. AdS_D space has the isometry group $\mathrm{SO}(2;D)$.

Global coordinates:

$$X^{d+1} = R\sqrt{1+\rho^2}\,\cos t\,, \qquad X^0 = R\sqrt{1+\rho^2}\,\sin t\,, \tag{B.3}$$
$$X^1 = R\rho\cos\theta_1\,, \qquad X^2 = R\rho\sin\theta_1\cos\theta_2\,, \tag{B.4}$$
$$X^3 = R\rho\sin\theta_1\sin\theta_2\,, \qquad X^d = R\rho\sin\theta_1\sin\theta_2\ldots\sin\theta_{d-1}\,. \tag{B.5}$$

The induced metric in these coordinates takes the form

$$\mathrm{d}s^2 = -(1+\rho^2)\,\mathrm{d}t^2 + \frac{\mathrm{d}\rho^2}{1+\rho^2} + \rho^2\Omega_{d-1}^2\,. \tag{B.6}$$

Here, Ω_{d-1}^2 is the metric on the $(d-1)$-dimensional unit sphere, $R = 1$. These spherical coordinates are the global coordinates: $\rho > 0$ and t have a period of 2π (the covering space can also be considered). The introduction of $\rho = \sinh r$ leads to

$$\mathrm{d}s^2 = -\cosh^2 r\,\mathrm{d}t^2 + \mathrm{d}r^2 + \sinh^2 r\Omega_{d-1}^2\,. \tag{B.7}$$

Poincaré coordinates, $R = 1$:

$$X^1 = \frac{x^1}{z}\,, \quad \ldots \quad X^{d-1} = \frac{x^{d-1}}{z}\,, \qquad X^{d+1} = \frac{x^0}{z}\,,$$
$$X^d = \frac{z^2 - 1 - (x^0)^2 + (x^1)^2 + \ldots + (x^{d-1})^2}{2z}\,, \tag{B.8}$$
$$X^0 = \frac{z^2 + 1 - (x^0)^2 + (x^1)^2 + \ldots + (x^{d-1})^2}{2z}\,,$$

where it is assumed that $z > 0$. These coordinates cover only part of AdS_D space. Metric (B.2) in (B.8) coordinates is written down as

$$\mathrm{d}s^2 = \frac{R^2}{z^2}(-\mathrm{d}\tau^2 + \mathrm{d}\mathbf{x}^2 + \mathrm{d}z^2)\,. \tag{B.9}$$

Figure 12a depicts AdS space in the form of a cylinder. The time is directed vertically upward, and the side surface of the cylinder makes up the boundary. $\mathrm{R}\times\mathrm{S}^1$ and $\mathrm{R}\times\mathrm{S}^3$ are the boundaries of AdS_3 and AdS_5 spaces, respectively. In Fig. 12b, SchAdS space is schematically represented as a cylinder with the event horizon in the form of the inner cylinder.

Figure 13a displays the planar limit of SchAdS space in the form of a flat space. The region shown as a green parallelepiped in Fig. 13a is enlarged in Fig. 13b. Here, both the boundary (blue) and the horizon (red) become planes. The flat space on which we 'live' is colored blue. Figure 13c presents a typical picture encountered in the discussion of AdS/CFT correspondence. The flat spacetime in which we live forms the boundary of AdS space. Correlators of the quantum field at points A and B at the boundary are given by the geodesic ending at these points and hanging down into the bulk. The presence of horizon deforms the geodesic.

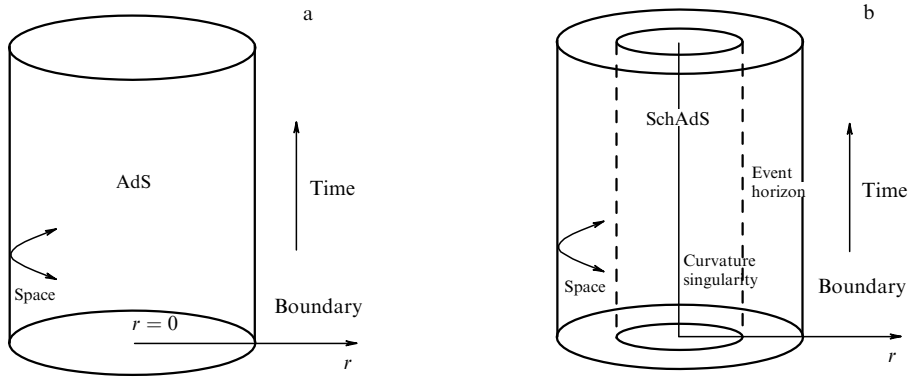

Figure 12. (a) Schematic of AdS space. (b) SchAdS space in the form of a cylinder. Event horizon depicted in the form of the inner cylinder.

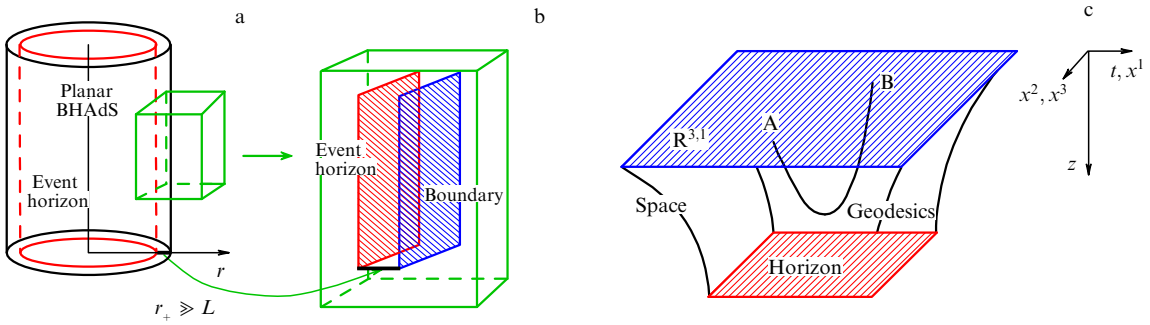

Figure 13. (Color online.) (a) Planar limit of SchAdS space. (b) The enlarged region shown as a green parallelepiped in figure (a). (c) Planar black hole in AdS space. The flat spacetime on which we 'live' is colored blue.

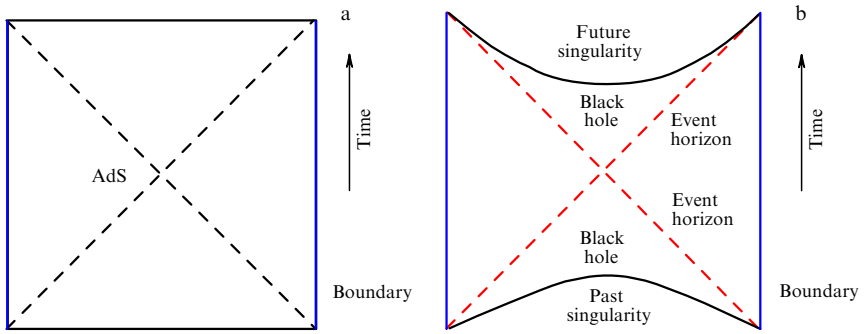

Figure 14. (a) Penrose diagram of AdS space. (b) Penrose diagram of AdS space with a black hole (SchAdS).

It is convenient to describe global properties in the global coordinates. Penrose diagrams of AdS and BHAdS spaces are presented in Figs 14a and 14b, respectively.

References

1. Adams J et al. (STAR Collab.) *Nucl. Phys. A* **757** 102 (2005)
2. Adcox K et al. (PHENIX Collab.) *Nucl. Phys. A* **757** 184 (2005)
3. Arsene I et al. (BRAHMS Collab.) *Nucl. Phys. A* **757** 1 (2005)
4. Back B B et al. *Nucl. Phys. A* **757** 28 (2005)
5. "Quark Matter 2011: Proc. of the 22nd Intern. Conf. on Ultra-Relativistic Nucleus–Nucleus Collisions, Annecy, France, 23–28 May 2011" *J. Phys. G Nucl. Part. Phys.* **38** (12) (2011)
6. Aamodt K et al. (ALICE Collab.) *Phys. Rev. Lett.* **105** 252301 (2010)
7. Masui H et al. *Nucl. Phys. A* **830** 463C (2009)
8. Shuryak E *Prog. Part. Nucl. Phys.* **53** 273 (2004)
9. Shuryak E *Nucl. Phys. A* **750** 64 (2005)
10. Heinz U W, hep-ph/0407360
11. Leonidov A V *Phys. Usp.* **48** 323 (2005); *Usp. Fiz. Nauk* **175** 345 (2005)
12. Salgado C A, arXiv:0907.1219
13. Dremin I M, Leonidov A V *Phys. Usp.* **53** 1123 (2010); *Usp. Fiz. Nauk* **180** 1167 (2010)
14. Gelis F *J. Phys. Conf. Ser.* **381** 012021 (2012); arXiv:1110.1544
15. Snellings R *New J. Phys.* **13** 055008 (2011); arXiv:1102.3010
16. Gyulassy M, McLerran L *Nucl. Phys. A* **750** 30 (2005); nucl-th/0405013
17. Alford M G et al. *Rev. Mod. Phys.* **80** 1455 (2008); arXiv:0709.4635
18. Sorensen P, arXiv:1201.0784
19. Iancu E, arXiv:1205.0579
20. Maldacena J M *Adv. Theor. Math. Phys.* **2** 231 (1998)
21. Gubser S S, Klebanov I R, Polyakov A M *Phys. Lett. B* **428** 105 (1998)
22. Witten E *Adv. Theor. Math. Phys.* **2** 253 (1998)
23. Aharony O et al. *Phys. Rep.* **323** 183 (2000)
24. Casalderrey-Solana J et al., arXiv:1101.0618
25. Landau L D *Izv. Akad. Nauk SSSR Ser. Fiz.* **17** 51 (1953)

26. Fermi E *Prog. Theor. Phys.* **5** 570 (1950)
27. Pomeranchuk I Ya *Dokl. Akad. Nauk SSSR* **78** 884 (1951)
28. Aref'eva I Ya, Slavnov A A "Teoriya kalibrovochnykh polei" ("Gauge field theory"), in *XIV Mezhdunarodnaya Shkola Molodykh Uchenykh po Fizike Vysokikh Energii, Dubna, 1980* (XIV Intern. School for Young Scientists on High Energy Physics, Dubna, 1980) (Dubna: JINR, 1981) p. 36
29. Snellings *J. Phys. Conf. Ser.* **381** 012019 (2012)
30. Martinez G, arXiv:1304.1452
31. Singh R et al. *Adv. High Energy Phys.* **2013** 761474 (2013); arXiv:1304.2969
32. Karsch F *Lecture Notes Phys.* **583** 209 (2002); hep-lat/0106019
33. Fortov V E *Phys. Usp.* **52** 615 (2009); *Usp. Fiz. Nauk* **179** 653 (2009)
34. Gorbunov D S, Rubakov V A *Introduction to the Theory of the Early Universe: Hot Big Bang Theory* (Singapore: World Scientific, 2011); Translated from Russian: *Vvedenie v Teoriyu Rannei Vselennoi: Teoriya Goryachego Bol'shogo Vzryva* (Moscow: LKI, 2008)
35. Flambaum V V, Shuryak E V *Europhys. Lett.* **74** 813 (2006); hep-th/0512038
36. Shuryak E *Prog. Part. Nucl. Phys.* **62** 48 (2009); arXiv:0807.3033
37. Feinberg E L *Phys. Usp.* **41** 617 (1998); *Usp. Fiz. Nauk* **168** 697 (1998)
38. Denisov D "Experimental Summary 2013", in *Rencontres de Moriond QCD and High Energy Interactions, La Thuile, March 9–16, 2013*; arXiv:1306.6908
39. Salgado C A, arXiv:0907.1219
40. Barannikova O (STAR Collab.), nucl-ex/0403014
41. Braun-Munzinger P, Redlich K, Stachel J, in *Quark Gluon Plasma* (Eds R C Hwa, X-N Wang) (Singapore: World Scientific Publ., 2004) p. 491
42. Adare A et al. (PHENIX Collab.) *Phys. Rev. Lett.* **104** 132301 (2010)
43. Peigné S, Smilga A V *Phys. Usp.* **52** 659 (2009); *Usp. Fiz. Nauk* **179** 697 (2009)
44. Matsui T, Satz H *Phys. Lett. B* **178** 416 (1986)
45. Kaczmarek O et al. *Phys. Rev. D* **70** 074505 (2004); *Phys. Rev. D* **72** 059903 (2005), Erratum
46. Petrov K (RBC-Bielefeld Collab.) *PoS LAT* **2006** 144 (2006)
47. Satz H *J. Phys. G Nucl. Part. Phys.* **32** R25 (2006)
48. Karsch F, Mehr M T, Satz H *Z. Phys. C* **37** 617 (1988)
49. Digal S, Petreczky P, Satz H *Phys. Rev. D* **64** 094015 (2001)
50. Mocsy A, Petreczky P *Phys. Rev. D* **73** 074007 (2006)
51. Mocsy A, Petreczky P *Phys. Rev. Lett.* **99** 211602 (2007)
52. Adare A et al. (PHENIX Collab.) *Phys. Rev. Lett.* **98** 232301 (2007)
53. Chatrchyan S et al. (CMS Collab.) *Phys. Rev. Lett.* **109** 222301 (2012)
54. Ollitrault J Y *Phys. Rev. D* **46** 229 (1992)
55. Wang X N *Phys. Rev. C* **63** 054902 (2001)
56. Gyulassy M et al. *Phys. Lett. B* **526** 301 (2002)
57. Gyulassy M, Vitev I, Wang X N *Phys. Rev. Lett.* **86** 2537 (2001)
58. Ali A, Kramer G *Eur. Phys. J. H* **36** 245 (2011)
59. Brodsky S J, de Téramond G, Karliner M *Annu. Rev. Nucl. Part. Sci.* **62** 1 (2012)
60. Gribov V N, Lipatov L N *Sov. J. Nucl. Phys.* **15** 675 (1972); *Yad. Fiz.* **15** 1218 (1972)
61. Dokshitser Yu L *Sov. Phys. JETP* **46** 641 (1977); *Zh. Eksp. Teor. Fiz.* **73** 1216 (1977)
62. Altarelli G, Parisi G *Nucl. Phys. B* **126** 298 (1977)
63. Muller B, Schafer A *Int. J. Mod. Phys. E* **20** 2235 (2011)
64. Bjorken J D *Phys. Rev. D* **27** 140 (1983)
65. Aamodt K et al. (ALICE Collab.) *Phys. Lett. B* **696** 328 (2011)
66. Hanbury Brown R, Twiss R *Nature* **178** 1046 (1956)
67. Lisa M A et al. *Annu. Rev. Nucl. Part. Sci.* **55** 357 (2005)
68. Petráň M, Rafelski J *Phys. Rev. C* **88** 021901(R) (2013); arXiv: 1303.0913
69. Aad G et al. (ATLAS Collab.) *Phys. Lett. B* **710** 363 (2012)
70. Back B B et al. *Phys. Rev. Lett.* **91** 052303 (2003)
71. Wong C Y *Phys. Rev. C* **78** 054902 (2008)
72. Steinberg P *Nucl. Phys. A* **752** 423 (2005)
73. Wong C Y *EPJ Web Conf.* **7** 01006 (2010)
74. Abbas E et al. (ALICE Collab.) *Phys. Lett. B* **726** 610 (2013); arXiv:1304.0347
75. Chatrchyan S et al. (CMS Collab.) *Phys. Rev. Lett.* **109** 152303 (2012)
76. Belen'kii S Z, Landau L D *Usp. Fiz. Nauk* **56** 309 (1955)
77. Khalatnikov I M *Zh. Eksp. Teor. Fiz.* **27** 529 (1954)
78. Rozental' I L *Sov. Phys. JETP* **4** 217 (1957); *Zh. Eksp. Teor. Fiz.* **31** 278 (1956)
79. Milekhin G A *Sov. Phys. JETP* **8** 682 (1959); *Zh. Eksp. Teor. Fiz.* **35** 978 (1958)
80. Liao J, Koch V *Phys. Rev. C* **80** 034904 (2009)
81. Teaney D, Lauret J, Shuryak E V *Phys. Rev. Lett.* **86** 4783 (2001)
82. Huovinen P et al. *Phys. Lett. B* **503** 58 (2001)
83. Kolb P F et al. *Nucl. Phys. A* **696** 197 (2001)
84. Hirano T, Tsuda K *Phys. Rev. C* **66** 054905 (2002)
85. Kolb P F, Heinz U W, in *Quark Gluon Plasma* (Eds R C Hwa, X-N Wang) (Singapore: World Scientific Publ., 2004) p. 634
86. Teaney D A, arXiv:0905.2433
87. Janik R A, Peschanski R B *Phys. Rev. D* **73** 045013 (2006)
88. Gubser S S *Phys. Rev. D* **82** 085027 (2010)
89. Gubser S S, Yarom A *Nucl. Phys. B* **846** 469 (2011)
90. Staig P, Shuryak E *Phys. Rev. C* **84** 034908 (2011)
91. Staig P, Shuryak E *Phys. Rev. C* **84** 044912 (2011)
92. Gubser S S *Phys. Rev. C* **87** 014909 (2013)
93. DeWolfe O et al. *Prog. Part. Nucl. Phys.* **75** 86 (2014); arXiv: 1304.7794
94. Lappi T, McLerran L *Nucl. Phys. A* **772** 200 (2006)
95. Eckart C *Phys. Rev.* **58** 919 (1940)
96. Landau L D, Lifshitz E M *Fluid Mechanics* (Oxford: Pergamon Press, 1987); Translated from Russian: *Gidrodinamika* (Moscow: Nauka, 1986)
97. Israel W *Ann. Physics* **100** 310 (1976)
98. Stewart J *Proc. R. Soc. Lond. A* **357** 59 (1977)
99. Israel W, Stewart J M *Ann. Physics* **118** 341 (1979)
100. Liu I-Sh, Müller I, Ruggeri T *Ann. Physics* **169** 191 (1986)
101. Baier R et al. *JHEP* (04) 100 (2008)
102. Bhattacharyya S et al. *JHEP* (02) 045 (2008)
103. Hubeny V E, Minwalla S, Rangamani M, arXiv:1107.5780
104. Hiscock W A, Lindblom L *Ann. Physics* **151** 466 (1983)
105. Pu S, Koide T, Rischke D H *Phys. Rev. D* **81** 114039 (2010)
106. Gale C, Jeon S, Schenke B *Int. J. Mod. Phys. A* **28** 1340011 (2013)
107. Betz B, Henkel D, Rischke D H *J. Phys. G Nucl. Part. Phys.* **36** 064029 (2009)
108. Muronga A *Phys. Rev. Lett.* **88** 062302 (2002); *Phys. Rev. Lett.* **89** 159901 (2002), Erratum
109. Denicol G S et al. *Eur. Phys. J. A* **48** 170 (2012); arXiv:1206.1554
110. Florchinger S, Wiedemann U A *JHEP* (11) 100 (2011)
111. Romatschke P *Eur. Phys. J. C* **52** 203 (2007)
112. Romatschke P, Romatschke U *Phys. Rev. Lett.* **99** 172301 (2007)
113. Luzum M, Romatschke P *Phys. Rev. C* **78** 034915 (2008); *Phys. Rev. C* **79** 039903 (2009), Erratum
114. Heinz U W, Song H, Chaudhuri A K *Phys. Rev. C* **73** 034904 (2006)
115. Song H, Heinz U W *Phys. Lett. B* **658** 279 (2008)
116. Song H, Heinz U W *Phys. Rev. C* **78** 024902 (2008)
117. Grmela M, Ottinger H C *Phys. Rev. E* **56** 6620 (1997)
118. Dusling K, Teaney D *Phys. Rev. C* **77** 034905 (2008)
119. Schenke B, Jeon S, Gale C *Phys. Rev. Lett.* **106** 042301 (2011)
120. Schenke B, Jeon S, Gale C *Phys. Lett. B* **702** 59 (2011)
121. Bozek P *Phys. Rev. C* **85** 034901 (2012)
122. Denicol G S et al. *Phys. Rev. C* **80** 064901 (2009)
123. Monnai A, Hirano T *Phys. Rev. C* **80** 054906 (2009)
124. Song H, Heinz U *Phys. Rev. C* **81** 024905 (2010)
125. Paech K, Pratt S *Phys. Rev. C* **74** 014901 (2006)
126. Kharzeev D, Tuchin K *JHEP* (09) 093 (2008)
127. Meyer H B *Nucl. Phys. A* **830** 641c (2009)
128. Buchel A *Phys. Lett. B* **681** 200 (2009)
129. El A, Xu Z, Greiner C *Phys. Rev. C* **81** 041901 (2010)
130. Heinz U W, Snellings R *Annu. Rev. Nucl. Part. Sci.* **63** 123 (2013); arXiv:1301.2826
131. Martinez M, Strickland M *Nucl. Phys. A* **848** 183 (2010)
132. Martinez M, Strickland M *Nucl. Phys. A* **856** 68 (2011)
133. Florkowski W, Ryblewski R *Phys. Rev. C* **83** 034907 (2011)
134. Ryblewski R, Florkowski W *Eur. Phys. J. C* **71** 1761 (2011)
135. Peschanski R, Saridakis E N *Nucl. Phys. A* **849** 147 (2011)
136. Martinez M, Ryblewski R, Strickland M *Phys. Rev. C* **85** 064913 (2012)
137. Ollitrault J Y *Eur. J. Phys.* **29** 275 (2008)

138. Miller M L et al. *Annu. Rev. Nucl. Part. Sci.* **57** 205 (2007)
139. Teaney D A, arXiv:0905.2433
140. Hirano T, van der Kolk N, Bilandzic A *Lecture Notes Phys.* **785** 139 (2010)
141. Luzum M, Ollitrault J-Y *Nucl. Phys. A* **904–905** 377 (2013); arXiv:1210.6010
142. Peschanski R, Saridakis E N *Phys. Rev. C* **80** 024907 (2009)
143. Khalatnikov I M, Kamenshchik A Y *Phys. Lett. A* **331** 12 (2004)
144. Kovtun P, Son D T, Starinets A O *Phys. Rev. Lett.* **94** 111601 (2005)
145. Heller M P, Janik R A, Peschanski R *Acta Phys. Polon. B* **39** 3183 (2008)
146. Berges J et al. *Phys. Rev. D* **89** 074011 (2014); arXiv:1303.5650
147. Nakamura A, Sakai S *Phys. Rev. Lett.* **94** 072305 (2005)
148. Meyer H B *Phys. Rev. D* **76** 101701 (2007)
149. Alver B et al. (PHOBOS Collab.) *Phys. Rev. Lett.* **98** 242302 (2007)
150. Alver B H et al. *Phys. Rev. C* **82** 034913 (2010)
151. Alver B, Roland G *Phys. Rev.* **C81** 054905 (2010)
152. Schenke B, Jeon S, Gale C *Phys. Rev. Lett.* **106** 042301 (2011)
153. Qiu Z, Heinz U W *Phys. Rev. C* **84** 024911 (2011)
154. Gale C et al. *Phys. Rev. Lett.* **110** 012302 (2013)
155. Iancu E, Venugopalan R, in *Quark Gluon Plasma* (Eds R C Hwa, X-N Wang) (Singapore: World Scientific Publ., 2004) p. 249
156. Gelis F *Nucl. Phys. A* **854** 10 (2011)
157. Schenke B, Tribedy P, Venugopalan R *Phys. Rev. Lett.* **108** 252301 (2012)
158. Schenke B, Tribedy P, Venugopalan R *Phys. Rev. C* **86** 034908 (2012)
159. Cleymans J *Pramana* **60** 787 (2003)
160. Steinberg P *Acta Phys. Hung. A* **24** 51 (2005)
161. Steinberg P *PoS CPOD* **2006** 036 (2006)
162. Allton C R et al. *Phys. Rev. D* **71** 054508 (2005)
163. Huovinen P, Petreczky P, Schmidt C *Central Eur. J. Phys.* **10** 1385 (2012)
164. Miao C, Schmidt C (RBC-Bielefeld Collab.) *PoS LATTICE2008* **172** (2008)
165. Cheng M et al. *Phys. Rev. D* **79** 074505 (2009)
166. Borsanyi S et al. *JHEP* (11) 077 (2010); arXiv:1007.2580
167. Policastro G, Son D T, Starinets A O *Phys. Rev. Lett.* **87** 081601 (2001)
168. Policastro G, Son D T, Starinets A O *JHEP* (09) 043 (2002)
169. Kovtun P, Son D T, Starinets A O *JHEP* (10) 064 (2003)
170. Heller M P, Janik R A *Phys. Rev. D* **76** 025027 (2007)
171. Buchel A *Phys. Rev. D* **85** 066004 (2012)
172. Keldysh L V *Sov. Phys. JETP* **20** 1018 (1965); *Zh. Eksp. Teor. Fiz.* **47** 1515 (1964)
173. Czajka A, Mrowczynski S *Phys. Rev. D* **86** 025017 (2012)
174. Aref'eva I Ya, Volovich I V *Phys. Lett. B* **433** 49 (1998)
175. de Haro S, Solodukhin S N, Skenderis K *Commun. Math. Phys.* **217** 595 (2001)
176. Vladimirov V S *Equations of Mathematical Physics* (New York: M. Dekker, 1971); Translated from Russian: *Uravneniya Matematicheskoi Fiziki* (Moscow: Nauka, 1981)
177. Gel'fand I M, Shilov G E *Obobshchennye Funktsii i Deistviya nad Nimi* (Generalized Functions and Actions on Them) (Moscow: Gos. Izd. Fiz.-Mat. Lit., 1958)
178. Fronsdal C *Phys. Rev. D* **20** 848 (1979)
179. Vasil'ev M A *Phys. Usp.* **46** 218 (2003); *Usp. Fiz. Nauk* **173** 226 (2003)
180. Vasiliev M A *Phys. Usp.* **54** 641 (2011); *Usp. Fiz. Nauk* **181** 665 (2011)
181. Fradkin E S, Vasiliev M A *Nucl. Phys. B* **291** 141 (1987)
182. Metsaev R R *Phys. Rev. D* **78** 106010 (2008)
183. Metsaev R R *Phys. Rev. D* **85** 126011 (2012)
184. Son D T, Starinets A O *JHEP* (09) 042 (2002)
185. Herzog C P, Son D T *JHEP* (03) 046 (2003)
186. Balasubramanian V, Ross S F *Phys. Rev. D* **61** 044007 (2000)
187. Hawking S W, Page D N *Commun. Math. Phys.* **87** 577 (1983)
188. Gubser S S, Klebanov I R, Peet A W *Phys. Rev. D* **54** 3915 (1996)
189. Fefferman C, Graham C R, in *Elie Cartan et les Mathématiques d'aujourd'hui, Lyon, 25 – 29, 1984* Astérisque (Paris: Société Mathématique de France, 1985) p. 95
190. Kovchegov Y V *Rep. Prog. Phys.* **75** 124301 (2012)
191. Bernamonti A, Peschanski R *Nucl. Phys. B Proc. Suppl.* **216** 94 (2011)
192. Herzog C P et al. *JHEP* (07) 013 (2006)
193. Gubser S S *Phys. Rev. D* **74** 126005 (2006)
194. Janik R A, Peschanski R B *Phys. Rev. D* **74** 046007 (2006)
195. Chamblin A et al. *Phys. Rev. D* **60** 064018 (1999)
196. Mateos D et al. *JHEP* (11) 085 (2007)
197. Erdmenger J et al. *JHEP* (01) 055 (2009)
198. Kobayashi S et al. *JHEP* (02) 016 (2007)
199. Gursoy U, Kiritsis E *JHEP* (02) 032 (2008)
200. Gursoy U, Kiritsis E, Nitti F *JHEP* (02) 019 (2008)
201. Gursoy U et al. *Nucl. Phys. B* **820** 148 (2009)
202. Gursoy U et al. *JHEP* (12) 056 (2009)
203. Shirkov D V *Phys. Part. Nucl. Lett.* **7** 379 (2010)
204. Christodoulou D, Klainerman S *The Global Nonlinear Stability of the Minkowski Space* (Princeton: Princeton Univ. Press, 1993)
205. Friedrich H *Commun. Math. Phys.* **107** 587 (1986)
206. Bizon P, Rostworowski A *Phys. Rev. Lett.* **107** 031102 (2011)
207. Jalmuzna J, Rostworowski A, Bizon P *Phys. Rev. D* **84** 085021 (2011)
208. Dias Ó J C, Horowitz G T, Santos J E *Class. Quantum Grav.* **29** 194002 (2012)
209. Garfinkle D, Pando Zayas L A *Phys. Rev. D* **84** 066006 (2011)
210. Garfinkle D et al. *JHEP* (02) 119 (2012)
211. Chandrasekhar S, Detweiler S L *Proc. R. Soc. Lond. A* **344** 441 (1975)
212. Horowitz G T, Hubeny V E *Phys. Rev. D* **62** 024027 (2000)
213. Starinets A O *Phys. Rev. D* **66** 124013 (2002)
214. Kovtun P K, Starinets A O *Phys. Rev. D* **72** 086009 (2005)
215. Friess J J et al. *JHEP* (04) 080 (2007)
216. Iqbal N, Liu H *Phys. Rev. D* **79** 025023 (2009)
217. Hubeny V E, Rangamani M *Adv. High Energy Phys.* **2010** 297916 (2010)
218. Hawking S W, Ellis G R E *The Large Scale Structure of Space–Time* (Cambridge: Cambridge Univ. Press, 1973)
219. Wald R M *General Relativity* (Chicago: Univ. of Chicago Press, 1984)
220. Penrose R, unpublished (1974)
221. Gubser S A, Pufu S S, Yarom A *Phys. Rev. D* **78** 066014 (2008)
222. Gubser S S, Pufu S S, Yarom A *JHEP* (11) 050 (2009)
223. Grumiller D, Romatschke R *JHEP* (08) 027 (2008)
224. Alvarez-Gaume L et al. *JHEP* (02) 009 (2009)
225. Albacete J L, Kovchegov Y V, Taliotis A *JHEP* (07) 100 (2008)
226. Lin S, Shuryak E *Phys. Rev. D* **79** 124015 (2009)
227. Lin S, Shuryak E *Phys. Rev. D* **83** 045025 (2011)
228. Albacete J L, Kovchegov Y V, Taliotis A *JHEP* (05) 060 (2009)
229. Aref'eva I Ya, Bagrov A A, Guseva E A *JHEP* (12) 009 (2009)
230. Aref'eva I Ya, Bagrov A A, Joukovskaya L V *JHEP* (03) 002 (2010)
231. Kovchegov Y V, Lin S *JHEP* (03) 057 (2010)
232. Kiritsis E, Taliotis A *JHEP* (04) 065 (2012)
233. Chesler P M, Yaffe L G *Phys. Rev. Lett.* **106** 021601 (2011)
234. Aref'eva I Ya, Bagrov A A, Pozdeeva E O *JHEP* (05) 117 (2012)
235. Taliotis A *JHEP* (05) 034 (2013)
236. Danielsson D H, Keski-Vakkuri E, Kruczenski M *Nucl. Phys. B* **563** 279 (1999)
237. Hubeny V E, Rangamani M, Takayanagi T *JHEP* (07) 062 (2007)
238. Balasubramanian V et al. *Phys. Rev. Lett.* **106** 191601 (2011)
239. Balasubramanian V et al. *Phys. Rev. D* **84** 026010 (2011)
240. Abajo-Arrastia J, Aparicio J, Lopez E *JHEP* (11) 149 (2010)
241. Callan R, He J-Y, Headrick M *JHEP* (06) 081 (2012)
242. Galante D, Schvellinger M *JHEP* (07) 096 (2012)
243. Caceres E, Kundu A *JHEP* (09) 055 (2012)
244. Arefeva I Ya, Volovich I V *Theor. Math. Phys.* **174** 186 (2013); *Teor. Mat. Fiz.* **174** 216 (2013); arXiv: 1211.6041
245. Taylor M, arXiv:0812.0530
246. Tarrio J, Vandoren S *JHEP* (09) 017 (2011)
247. Keranen V, Keski-Vakkuri E, Thorlacius L *Phys. Rev. D* **85** 026005 (2012)
248. Keranen V, Thorlacius L *Class. Quantum Grav.* **29** 194009 (2012)
249. Aref'eva I, Bagrov A, Koshelev A S *JHEP* (07) 170 (2013); arXiv:1305.3267
250. Chesler P M, Yaffe L G *Phys. Rev. Lett.* **102** 211601 (2009)
251. Bhattacharyya S, Minwalla S *JHEP* (09) 034 (2009)

252. Arsiwalla X et al. *JHEP* (01) 144 (2011)
253. Das S R, Nishioka T, Takayanagi T *JHEP* (07) 071 (2010)
254. Hashimoto L, Iizuka N, Oka T *Phys. Rev. D* **84** 066005 (2011)
255. Volovich I V, Zagrebnov V A, Frolov V P *Theor. Math. Phys.* **29** 1012 (1976); *Teor. Mat. Fiz.* **29** 191 (1976)
256. Hotta M, Tanaka M *Class. Quantum Grav.* **10** 307 (1993)
257. Sfetsos K *Nucl. Phys. B* **436** 721 (1995)
258. Horowitz G T, Itzhaki N *JHEP* (02) 010 (1999)
259. Emparan R *Phys. Rev. D* **64** 024025 (2001)
260. Podolsky J, Griffiths J B *Class. Quantum Grav.* **15** 453 (1998)
261. Kang K, Nastase H *Phys. Rev. D* **72** 106003 (2005)
262. Aref'eva I Ya *Phys. Part. Nuclei* **41** 835 (2010)
263. Aref'eva I Ya *Int. J. Mod. Phys. B* **26** 1243010 (2012)
264. Heller M P, Janik R A, Witaszczyk P *Phys. Rev. Lett.* **108** 201602 (2012)
265. Eardley D M, Giddings S B *Phys. Rev. D* **66** 044011 (2002)
266. Bantilan H, Pretorius F, Gubser S S *Phys. Rev. D* **85** 084038 (2012)
267. Klein K, Nystrand J *Phys. Rev. C* **60** 014903 (1999)
268. Adams J et al. (STAR Collab.) *Phys. Rev. C* **70** 031902 (2004)
269. Ochs S, Heinz U W *Phys. Rev. C* **54** 3199 (1996)
270. Gursoy U et al. *Phys. Rev. Lett.* **101** 181601 (2008)
271. Gouteraux B, Kiritsis E *JHEP* (12) 036 (2011); arXiv:1107.2116
272. Aref'eva I Ya, Pozdeeva E O, Pozdeeva T O *Theor. Math. Phys.* **176** 861 (2013); *Teor. Mat. Fiz.* **176** 35 (2013)
273. Casalderrey-Solana J et al. *Phys. Rev. Lett.* **111** 181601 (2013); arXiv:1305.4919
274. Loganayagam R *JHEP* (05) 087 (2008)
275. Haack M, Yarom A *JHEP* (10) 063 (2008)
276. Bhattacharyya S et al. *JHEP* (12) 116 (2008)
277. Heller M P, Janik R, Witaszczyk P *Phys. Rev. D* **85** 126002 (2012)
278. Horowitz G T, Hubeny V E *Phys. Rev. D* **62** 024027 (2000)
279. Janik R, Peschanski R *Phys. Rev. D* **74** 046007 (2006)
280. Janik R *Phys. Rev. Lett.* **98** 022302 (2007)
281. Booth I, Heller M P, Spalinski M *Phys. Rev. D* **80** 126013 (2009)
282. Lublinsky M, Shuryak E *Phys. Rev. C* **76** 021901 (2007)
283. Heller M P et al. *Phys. Rev. Lett.* **102** 041601 (2009)
284. Kinoshita S et al. *Prog. Theor. Phys.* **121** 121 (2009)
285. Heller M P, Janik R A, Witaszczyk P *Phys. Rev. Lett.* **110** 211602 (2013); arXiv:1302.0697
286. Lipatov L N *Sov. Phys. JETP* **45** 216 (1977); *Zh. Eksp. Teor. Fiz.* **72** 411 (1977)
287. Lublinsky M, Shuryak E *Phys. Rev. D* **80** 065026 (2009)
288. Arnowitt R L, Deser S, Misner C W *Gen. Relat. Grav.* **40** 1997 (2008)
289. Chesler P M, Yaffe L G *Phys. Rev. D* **82** 026006 (2010)
290. Beuf G et al. *JHEP* (10) 043 (2009)
291. Kovchegov Y V, Taliotis A, *Phys. Rev. C* **76** 014905 (2007)
292. Lin S, Shuryak E *Phys. Rev. D* **77** 085013 (2008)
293. Lin S, Shuryak E *Phys. Rev. D* **77** 085014 (2008)
294. Bhattacharyya S et al. *JHEP* (06) 055 (2008)
295. Figueras P et al. *JHEP* (04) 137 (2009)
296. Heller M P et al. *Phys. Rev. Lett.* **108** 191601 (2012)
297. Heller M P et al. *JHEP* (09) 026 (2013); arXiv:1304.5172
298. van der Schee W *Phys. Rev. D* **87** 061901(R) (2013); arXiv:1211.2218
299. Chatrchyan S et al. (CMS Collab.) *Phys. Lett. B* **718** 795 (2013)
300. Abelev B et al. (ALICE Collab.) *Phys. Lett. B* **719** 29 (2013)
301. Aad G et al. (ATLAS Collab.) *Phys. Rev. Lett.* **110** 182302 (2013); arXiv:1212.5198
302. Adare A et al. (PHENIX Collab.) *Phys. Rev. Lett.* **111** 212301 (2013); arXiv:1303.1794